INFORMATION TO USERS

This material was produced from a microfilm copy of the original document. While the most advanced technological means to photograph and reproduce this document have been used, the quality is heavily dependent upon the quality of the original submitted.

The following explanation of techniques is provided to help you understand markings or patterns which may appear on this reproduction.

1. The sign or "target" for pages apparently lacking from the document photographed is "Missing Page(s)". If it was possible to obtain the missing page(s) or section, they are spliced into the film along with adjacent pages. This may have necessitated cutting thru an image and duplicating adjacent pages to insure you complete continuity.

2. When an image on the film is obliterated with a large round black mark, it is an indication that the photographer suspected that the copy may have moved during exposure and thus cause a blurred image. You will find a good image of the page in the adjacent frame.

3. When a map, drawing or chart, etc., was part of the material being photographed the photographer followed a definite method in "sectioning" the material. It is customary to begin photoing at the upper left hand corner of a large sheet and to continue photoing from left to right in equal sections with a small overlap. If necessary, sectioning is continued again — beginning below the first row and continuing on until complete.

4. The majority of users indicate that the textual content is of greatest value, however, a somewhat higher quality reproduction could be made from "photographs" if essential to the understanding of the dissertation. Silver prints of "photographs" may be ordered at additional charge by writing the Order Department, giving the catalog number, title, author and specific pages you wish reproduced.

5. PLEASE NOTE: Some pages may have indistinct print. Filmed as received.

Xerox University Microfilms
300 North Zeeb Road
Ann Arbor, Michigan 48106

Downloaded from SHAREOK. Persistent Handle URL: https://hdl.handle.net/11244/3833

75-6511

DUDENHOEFFER, Arthur Wood, 1942-
THE THERMOPOWER OF DILUTE ALLOYS OF INDIUM.

The University of Oklahoma, Ph.D., 1974
Physics, solid state

Xerox University Microfilms, Ann Arbor, Michigan 48106

THIS DISSERTATION HAS BEEN MICROFILMED EXACTLY AS RECEIVED.

THE UNIVERSITY OF OKLAHOMA

GRADUATE COLLEGE

THE THERMOPOWER OF DILUTE ALLOYS OF INDIUM

A DISSERTATION

SUBMITTED TO THE GRADUATE FACULTY

in partial fulfillment of the requirements for the

degree of

DOCTOR OF PHILOSOPHY

By

ARTHUR WOOD DUDENHOEFFER

Norman, Oklahoma

1974

THE THERMOPOWER OF DILUTE ALLOYS OF INDIUM

APPROVED BY

Ronald R. Bowrassa

Ronald Katouchi

R. A. Howard

S. E. Babb, Jr.

Robert Jay Blank

DISSERTATION COMMITTEE

ACKNOWLEDGMENT

The author expresses his sincere gratitude to Prof. R. R. Bourassa who suggested this work and guided its progress. His aid was invaluable in many aspects, particularly in the theoretical considerations involved and in the analysis of the data.

Appreciation is also expressed to Prof. S. E. Babb, who was always willing to lend his advice and help in the solution of a problem.

Thanks are expressed to Dr. Richard Moreland and Mr. Cliff Bettis for their assistance on various parts of the experiment, in particular the temperature controller.

Acknowledgment is made to the University of Oklahoma Instrument Shop personnel, who constructed most of the experimental apparatus, and to Mr. Ron Stermer, Glassblower, who helped in the preparation of the alloys.

A grant from the Research Corporation made preliminary work on this project possible.

The research was funded by the United States Atomic Energy Commission under Contract AT-(40-1)-3940.

The University of Oklahoma provided a graduate assistantship during 1970-72.

Finally, a word of appreciation is expressed to my parents, who have always encouraged me.

TABLE OF CONTENTS

	Page
Acknowledgment	iii
List of Tables	vi
List of Figures	vii
Chapter	
I. INTRODUCTION	1
A. Purpose of This Experiment	1
B. Thermoelectricity	3
C. Thermopower of Pure Metals	4
D. The Thermopower of Indium and Its Alloys	6
II. EQUIPMENT AND EXPERIMENTAL PROCEDURE	9
A. Apparatus	9
B. Dewar System and Insert Frame	9
C. Cryostat	11
D. Sample Holder	15
E. Mounting the Sample	21
F. Temperature Controller	22
G. Calibration of the Germanium Resistance Thermometer	25
H. Sample Preparation	31
I. Measurement Procedure	34

TABLE OF CONTENTS (continued)

		Page
III.	THEORETICAL DEVELOPMENT	41
	A. Synopsis	41
	B. The Diffusion Thermopower	42
	C. Nielsen-Taylor Effect in Pure Metals	43
	D. The Effect of Impurities on the Diffusion Thermopower	50
	E. Nielsen-Taylor Theory for Alloys	55
	F. Phonon Drag Thermopower in Pure Metals	59
	G. The Effect of Impurities on the Phonon Drag Thermopower	66
IV.	RESULTS AND ANALYSIS	68
	A. Experimental Results	68
	B. Analysis of the Diffusion Component	98
	C. Analysis of the Phonon Drag Component	103
V.	DISCUSSION AND CONCLUSIONS	106
	A. Discussion of Thermopower Results	106
	B. Sources of Error	110
APPENDIX A		113
APPENDIX B		117
LIST OF REFERENCES		119

LIST OF TABLES

Table		Page
1.	Nielsen-Taylor Figure of Merit	2
2.	Alloy Components	32
3.	Composition of the Specimens	69
4.	Fitting Parameters	102
5.	Calculated Rayleigh Scattering Parameter Ratios . . .	109

LIST OF FIGURES

Figure		Page
1.	Thermopower of Polycrystalline Indium: Different Measurements	7
2.	Cryostat Mounting Head	13
3.	Sample Holder and Specimen	16
4.	Heater Block	18
5.	Block Diagram of Temperature Control Circuit	23
6.	Modified Controller Circuit of Moreland and Tuma	26
7.	Block Diagram Calibration Circuit for the Germanium Resistance Thermometer	28
8.	Block Diagram of Circuit for Measuring Thermoelectric Potentials	35
9.	Block Diagram of Circuit for Measuring the Resistance of the Sample	39
10.	Typical Electron-Phonon Scattering	45
11.	Graphs of the Functions $\psi_1(\frac{T}{\theta})$, $\psi_2(\frac{T}{\theta})$, and $\psi_3(\frac{T}{\theta})$	48
12.	Form of the Function $\xi T/\theta$	51
13.	Typical Electron-Impurity Scattering	56
14.	Electron-Phonon Scattering on a Free Electron Fermi Surface	60

LIST OF FIGURES (continued)

Figure Page

15. Idealized Thermopower of a Metal with Hole-Like Charge Carriers 63

16. Thermopower of 60 Grade Polycrystalline Indium as a Function of Temperature 70

17. Thermopower of the Alloy In + 0.1 At. % Tl vs Pure Indium 72

18. Thermopower of the Alloy In + 0.3 At. % Tl vs Pure Indium 74

19. Thermopower of the Alloy In + 0.1 At. % Sn vs Pure Indium 76

20. Thermopower of the Alloy In + 0.2 At. % Sn vs Pure Indium 78

21. Thermopower of the Alloy In + 0.3 At. % Sn vs Pure Indium 80

22. Thermopower of the Alloy In + 0.1 At. % Cd vs Pure Indium 82

23. Thermopower of the Alloy In + 0.3 At. % Cd vs Pure Indium 84

24. Thermopower of the Alloy In + 0.1 At. % Pb vs Pure Indium 86

25. Thermopower of the Alloy In + 0.3 At. % Pb vs Pure Indium 88

26. Thermopower of the Alloy In + 0.1 At. % Ga vs Pure Indium 90

LIST OF FIGURES (continued)

Figure		Page
27.	Thermopower of the Alloy In + 0.3 At. % Ga vs Pure Indium	92
28.	Thermopower of the Alloy In + 0.3 At. % Mg vs Pure Indium	94
29.	Thermopower of the Alloy In + 0.1 At. % Zn vs Pure Indium	96
A1.	Graph of ΔS of In + 0.3 Atomic % Sn vs In Showing Correction Factor	114

I. INTRODUCTION

A. Purpose of This Experiment

The purpose of this dissertation is to discuss an experimental investigation of a new theory of electron diffusion thermopower introduced in 1968 by Nielsen and Taylor.[1,2,3,4] A figure of merit for the effect in various metals has been devised and is given in Column 7 of Table 1. Lead, indium, thallium, and aluminum have the highest ranking and thus should show the largest "Nielsen-Taylor" effect. (The calculation of this table is discussed in Chapter III.) Dudenhoeffer and Bourassa have completed investigations for the effect in dilute alloys of aluminum[5] and lead,[6] but no work has been done on thallium. Definite conclusions as to the validity of the theory are hampered by the complex nature of the competing process known as "phonon-drag," but the experimental data to date is consistent with the Nielsen-Taylor theory. Rybka and Bourassa[7] have found similar results for the case of vacancies in aluminum. In this work the case of dilute alloys of indium is discussed.

Most analyses of experimental work in the thermopower of metals is based on a separation of the electron diffusion thermopower from the phonon-drag component. Thus it is important that an effort be made to understand the role played by this new theory of electron dif-

Table 1. Nielsen-Taylor Figure of Merit

Metal	Valence	Pseudopotential (ryd)	Fermi Energy (ryd)	Debye Temp. (K)	Mass Ratio (M/m)	Figure of Merit	Rank
K	1	.09517	.1504	91	64803	3.15	6
Na	1	.12091	.2310	158	32239	4.10	5
Cu	1	.4588	.5169	343	77222	3.08	7
Ag	1	.3260	.4045	225	196647	1.56	11
Cd	2	.27844	.5577	209	273207	1.35	12
Mg	2	.26354	.5288	400	33324	2.71	9
Zn	2	.33521	.7076	327	132410	1.74	10
Al	3	.40182	.8599	428	30742	5.82	4
In	3	.32258	.6344	111	161013	9.77	2
Tl	3	.32066	.3992	78	323971	6.08	3
Sn	4	.36444	.7468	210	180310	3.02	8
Pb	4	.35091	.6996	105	179861	10.93	1

fusion thermopower.

A brief review of the concepts of thermoelectricity follows.

B. Thermoelectricity

In a metal there are three thermoelectric phenomena which are observed experimentally: the Peltier effect, the Thomson effect, and the Seebeck effect. If an electric current passes through a junction connecting two different metals (or the same metal in two different states), reversible heat is emitted or absorbed at the junction, depending on the direction of the current. This is the Peltier effect, and it comes about because the heat current density associated with the electric current density is a function of the particular conductor.

The rate that heat is generated per unit volume in a conductor depends on the electric current density in two ways. The irreversible Joule heating is proportional to the square of the current density. Another contribution is proportional to the product of the current density with the temperature gradient, and this heat may be emitted or absorbed, depending on the relative direction of the current and the temperature gradient. This Thomson effect can be observed experimentally by employing very small currents, for which the Thomson heat dominates the Joule heat.

If a temperature gradient is maintained across a conductor, then there exists an electric potential difference which for the given conductor is a function of the temperatures of the end points. This Seebeck effect may be written differentially as

$$dV = SdT, \tag{1}$$

where dV is the differential change in potential over an element of conductor, while dT is the change in temperature over the same element. The total change in potential may be found by integrating Equation (1) between the temperatures of the end points. The quantity S is called the Seebeck coefficient or the thermoelectric power or the thermopower. In general it is a function of material and of temperature.

The three thermoelectric phenomena are not independent and may be written in terms of each other by means of the Kelvin relations. There are excellent discussions of this and of many other facets of thermoelectricity in the book by MacDonald[8] and in the review article by Huebener.[9]

C. Thermopower of Pure Metals

Experimentally, above the Debye temperature the thermopower of many metals tends to be linear in temperature T with positive or negative slope, depending on the metal, i.e., $S \propto T$. Theoretically, a standard quasi-free electron analysis of the thermopower S_e due to the diffusion of charge carriers along the temperature gradient indicates that this should also be the case all the way down to absolute zero. What one actually observes in most cases is a thermopower with peaks or valleys or both, which may depart substantially from theoretical prediction. See, for example, MacDonald.[8]

In order to account for the observed behavior, the concept of phonon drag is usually invoked. Since a temperature gradient must

exist for a thermoelectric potential to be observed, the crystal lattice is not in thermal equilibrium. A lattice heat flux must be present, and the "phonons" which comprise this flux exert a force on the conduction electrons, thus giving rise to an additional contribution S_g to the thermopower. The total thermopower is then the sum of the two components:

$$S = S_e + S_g. \tag{2}$$

Unfortunately, no one has yet been able to devise an experiment which can measure the electronic diffusion thermopower and the phonon drag thermopower separately. One always measures the total. But theory does make some statements about how the phonon drag thermopower should behave, and these can be checked against experiment. This will be discussed more fully later.

In their new theory of thermopower Nielsen and Taylor[1,2,3,4] examine the electron diffusion contribution, employing a method roughly analagous to that which Kondo[10] used to explain the resistance minimum in metals at low temperature. Their results suggest that the departures of the thermopower from linearity may be explained in part through the diffusion component itself.

One way of investigating the validity of the various theories is to observe the effect of adding scattering centers to the crystal lattice. These centers may be impurities, vacancies, or any other lattice defect. Each theory makes certain predictions about the effect of alloying, and these can be checked against the experimental results. This is the procedure that has been adopted in this investigation.

D. The Thermopower of Indium and Its Alloys

There has been very little work done on indium.[11,12] This may be due to the fear that because indium has a non-cubic (tetragonal) crystal structure, polycrystalline samples might exhibit thermopower properties which are sample- and history-dependent. This would be a drawback if one's purpose were to construct a standard for comparison purposes. However, examination of the published data shows that the thermopower of most metals is sample- and history-dependent to some extent.

In any event polycrystalline indium should exhibit a thermopower, the main features of which are representative of any indium sample of comparative purity. This is illustrated by comparing the data of Figure 1. The full curve is from Bosacchi and Huebener[12] while the points represent two different samples from the present study. It should be noted that the sample of Bosacchi and Huebener was apparently of lesser purity than the other two.

Preliminary analysis using the Nielsen-Taylor theory predicted that the change in the diffusion components of thermopower on alloying indium should be strongly dependent on the particular impurity used. In fact, the theory predicted that this change should be more pronounced in indium than in any other metal except lead.

Figure 1. Thermopower of Polycrystalline Indium: Different Measurements.

o and + : This work.

——: Reference 12.

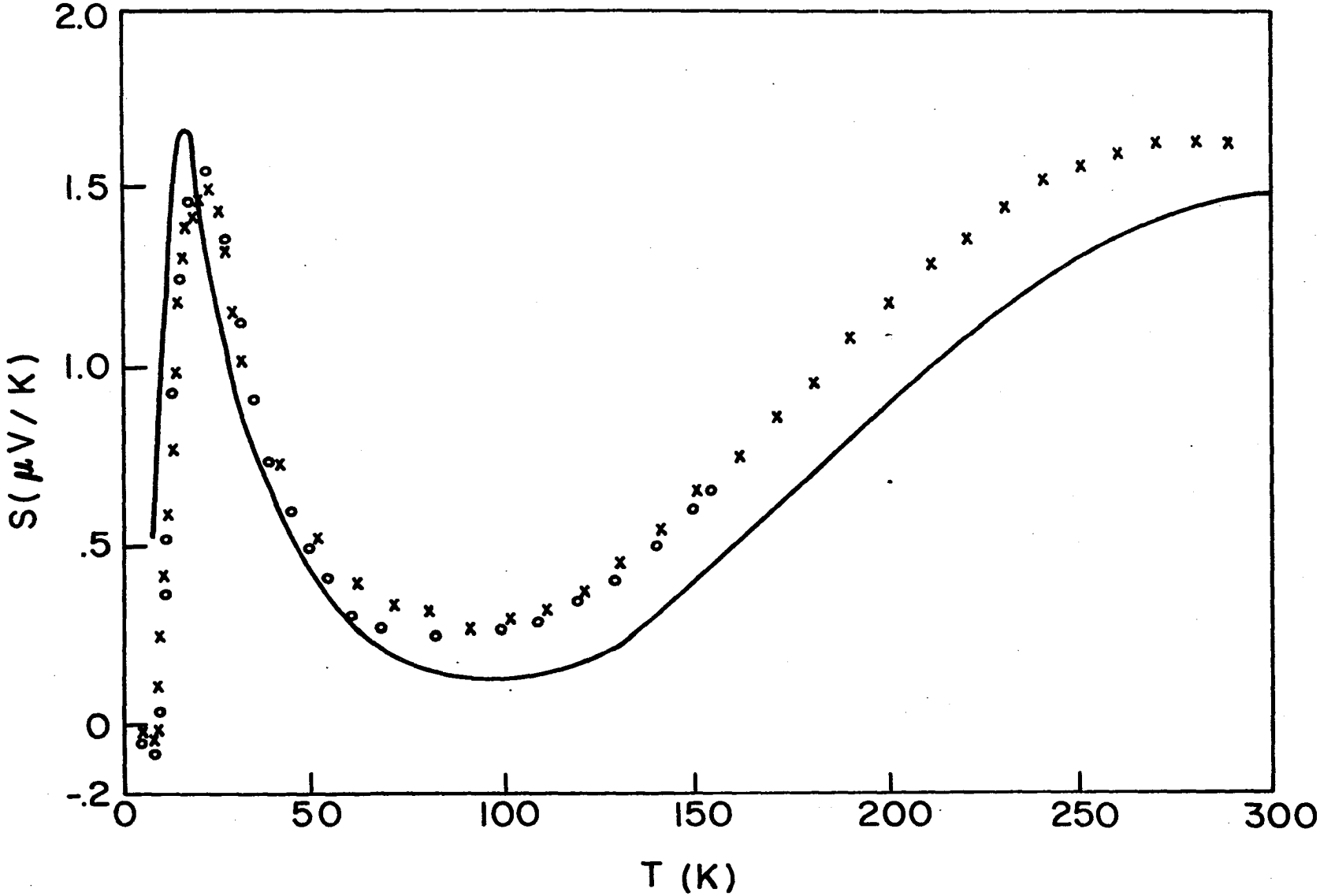
2.0
1.5
1.0
.5
0
-.2
S(μV/K)
0
50
100
150
200
250
300
T (K)

II. EQUIPMENT AND EXPERIMENTAL PROCEDURE

A. Apparatus

The experiments were performed using the following apparatus: a liquid helium Dewar system appropriately mounted, an insert frame carrying electrical leads and a pump line to the lower part of the helium Dewar where the experiments were performed, a cryostat consisting of a sample holder enclosed by a vacuum can, necessary pumps for the Dewar and the cryostat, a temperature controller employing either a germanium or a platinum resistance thermometer, a battery bank used as a source of direct current, and various measuring instruments (potentiometers, galvanometer, etc.). Either liquid helium or liquid nitrogen was used as a cryogenic bath.

B. Dewar System and Insert Frame

The Dewar system used has been described in detail elsewhere.[13] It consisted of two coaxially mounted cylindrical Pyrex Dewars, manufactured by Scientific Glass Blowing, Inc. of Houston, Texas. The vacuum jacket of the inner Dewar was connected through a valve to a pump and could be evacuated or filled with nitrogen gas as desired. The inner Dewar was mounted so that its chamber could be evacuated in preparation for the transfer of liquid helium into it when the

experiment was in place. Liquid nitrogen was placed in the outer Dewar to pre-cool the system before the transfer of the liquid helium.

A demountable insert frame constructed from 3/16 in diameter thin-walled stainless steel tubing and supporting cross vanes carried electrical leads and a pump line from the top of the Dewar system to near the bottom of its inner chamber where the experiments were performed. This frame is described in detail by Rybka.[13] The top of the frame consisted of a brass plate with filling port, vent, and vacuum and electrical feed-throughs. When the frame was in place for an experiment, this plate rested against a vacuum seal (rubber gasket) on a copper collar above the inner Dewar. Thus the inner chamber could be evacuated and filled with helium gas prior to the transfer of the liquid helium.

The cryostat was mounted at the insert frame's lower end, which consisted of a flat brass plate. The vacuum seal between the frame and the cryostat was made using an indium gasket.

The successful transfer of liquid helium from a storage container into the inner Dewar is something of an art. Assuming that all the equipment necessary to the transfer is in good working order, one can expect an efficient transfer if a) the Dewar is pre-cooled to near liquid nitrogen temperature, and b) the liquid helium is deposited low inside the chamber so that its rising vapors may cool the parts of the cryostat and insert frame above the liquid level. The following procedure was employed successfully for the Dewar system described.

1) With the insert frame and cryostat in place, begin evacua-

tion of the vacuum can.

2) Evacuate the jacket of the inner Dewar to about 0.01 torr of pressure; then fill it with nitrogen gas to about atmospheric pressure.

3) Evacuate the inner chamber to approximately 0.1 torr; then fill with helium gas.

4) Fill the outer Dewar with liquid nitrogen. Refill as necessary.

5) After sufficient time has elapsed (say overnight, or at least three hours) for the inner chamber to cool to near liquid nitrogen temperature, evacuate the vacuum jacket of the inner Dewar.

6) Flush the vacuum-jacketed transfer tube with helium gas.

7) Insert the ends of the transfer tube into the storage container and into the inner Dewar through the port on the top of the insert frame, respectively. Make sure the vent on the frame is free so the helium vapor may escape. Liquid helium should transfer under the pressure built up in the storage container. Extra pressure can be applied if necessary.

8) After the transfer is complete and the tube removed, cover the port and vent on the insert frame.

C. Cryostat

The cryostat was made up of three main parts: mounting head, vacuum can, and sample holder. It was similar in design to those described by Huebener[14] and Rybka.[13] The sample holder will be considered in a separate section.

Carrying electrical and vacuum lines, the cryostat mounting head, depicted in Figure 2, served as a connecting bridge between the insert frame above and the vacuum can below. It consisted basically of two circular brass plates 3 in apart, connected by three 3/16 in diameter thin-walled stainless steel support tubes equally spaced around the perimeter. A 3/8 in diameter tube served as the vacuum line. The lower plate accommodated two vacuum electrical feedthroughs as well as a liquid helium well for cooling the heat sink.

A vacuum seal was required at each plate. Indium gaskets were used for this purpose. The electrical feedthroughs in the bottom plate were a simplified version of those described by Anderson[15] and by Rybka.[13] Each feedthrough consisted of a copper sleeve, which was silver soldered to a 0.9 in length of 3/8 in diameter thin-walled stainless steel tubing. The copper sleeve was 0.6 in long, and about one half this length projected above the steel tube. This projection was tapered to a fine edge and etched in a solution of nitric acid.

Soft solder was used to mount the feedthroughs in the bottom plate of the head. This allowed for easy removal if it became necessary to change them at any time.

A thin phenolic disc rested against a stop in the middle of the copper sleeve. The disc contained holes to allow the passage of copper lead wires. With the phenolic disc and wire leads in place, the copper sleeve was potted with two coatings of an appropriate low-temperature epoxy. Stycast 2850 GT manufactured by Emerson & Cuming, Inc. was satisfactory for this purpose, but it was found that great care needed to be observed in the preparation of it.

Figure 2. Cryostat Mounting Head.

A. Upper brass vacuum plate.

B. Stainless steel frame.

C. Bakelite terminal strip.

D. Stainless steel pumping line.

E. Copper electrical leads.

F. Vacuum feedthrough (copper sleeve mounted on stainless steel base and potted with epoxy).

G. Lower brass plate containing screw connections to vacuum can.

H. Groove for crushing indium gasket.

I. Liquid helium (or nitrogen) well.

J. Heat sink (thermal ground).

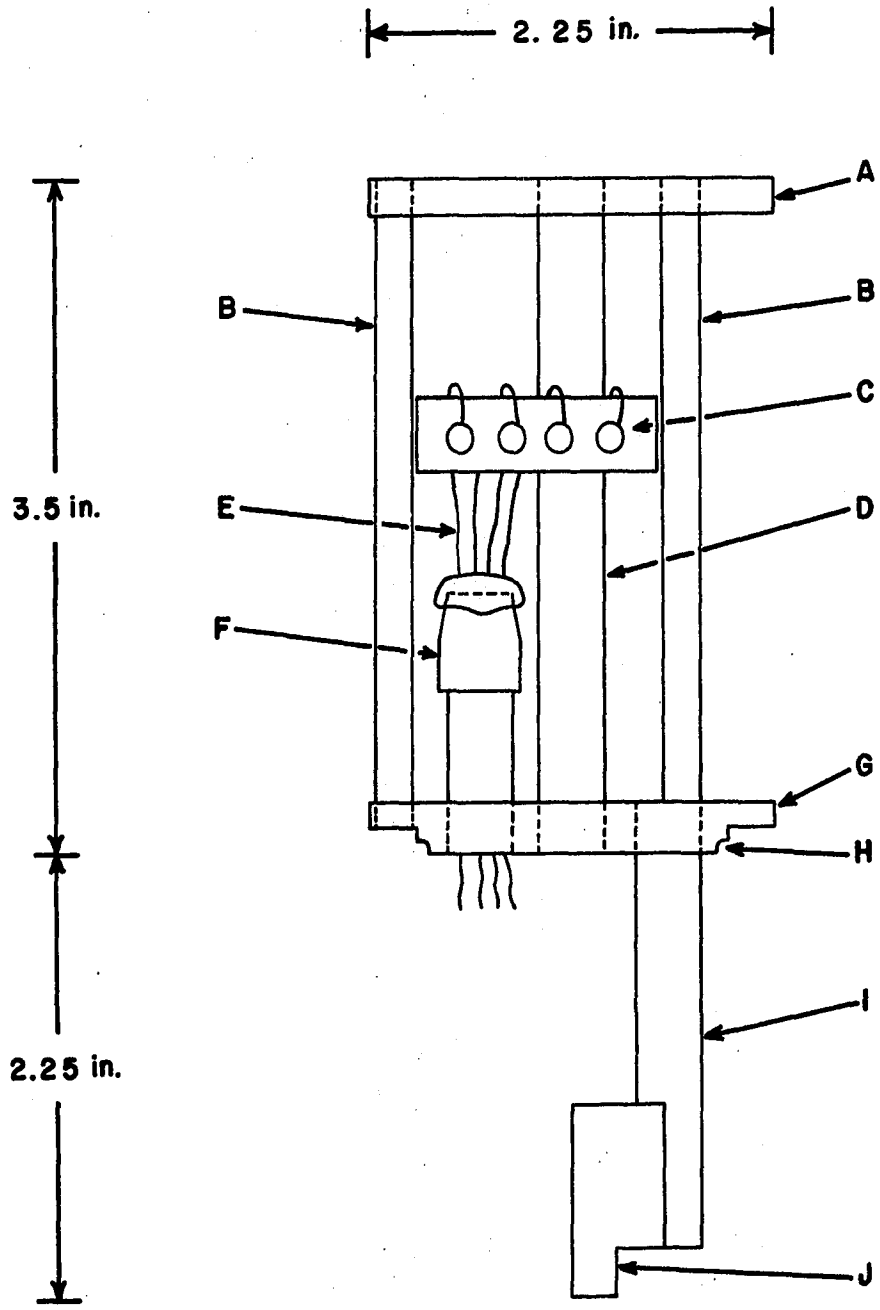
2.25 in.
3.5 in.
2.25 in.
A
B
B
C
D
E
F
G
H
I
J

Above the feedthroughs the lead wires were taken to terminal strips mounted around the perimeter of the head. Below the feedthroughs the wires were taken to various terminals mounted on the sample holder and on the bottom plate.

Extending below the bottom plate was the liquid helium well, which consisted of a hollow copper tube 1/4 in I.D. and length 2 in. Silver soldered to the end of this well was the copper heat sink or thermal ground. It was constructed such that liquid helium (or nitrogen) could flow into a cavity in it from the well. Thus efficient heat dissipation in the heat sink was assured.

The copper vacuum can was 7.75 in long and was of 1.50 in I.D. In situ it enclosed the helium well, heat sink, and sample holder. An estimated vacuum of 10^{-4} to 10^{-5} torr could be achieved at liquid helium temperature with the pumps available.

D. Sample Holder

The sample holder is shown in Figure 3. It was constructed from two pieces of 1/8 in diameter thin-walled stainless steel tubing, each 6.625 in long, held together at either end by a silver soldered brass fitting. Brass fittings near the top were used as interfaces to attach the sample holder to the heat sink with small screws. Terminal strips made of phenolic were attached to the brass end pieces with screws.

The copper heater block, depicted in Figure 4, was located near the bottom of the sample holder. It was bilateral with equal resistance winding on either side. The sample was placed between these

Figure 3. Sample Holder and Specimen.

A. Copper electrical leads: 1,2,3,4,5.

B. Brass end pieces.

C. Brass interface for connecting sample holder to heat sink.

D. Copper heat sink (thermal ground).

E. Thermoelectric reference (generally 69 grade pure indium).

F. Specimen (dilute alloy of indium).

G. Stainless steel frame.

H. Fitting for thermocouple block if desired.

I. Heater block.

J. Hot junction.

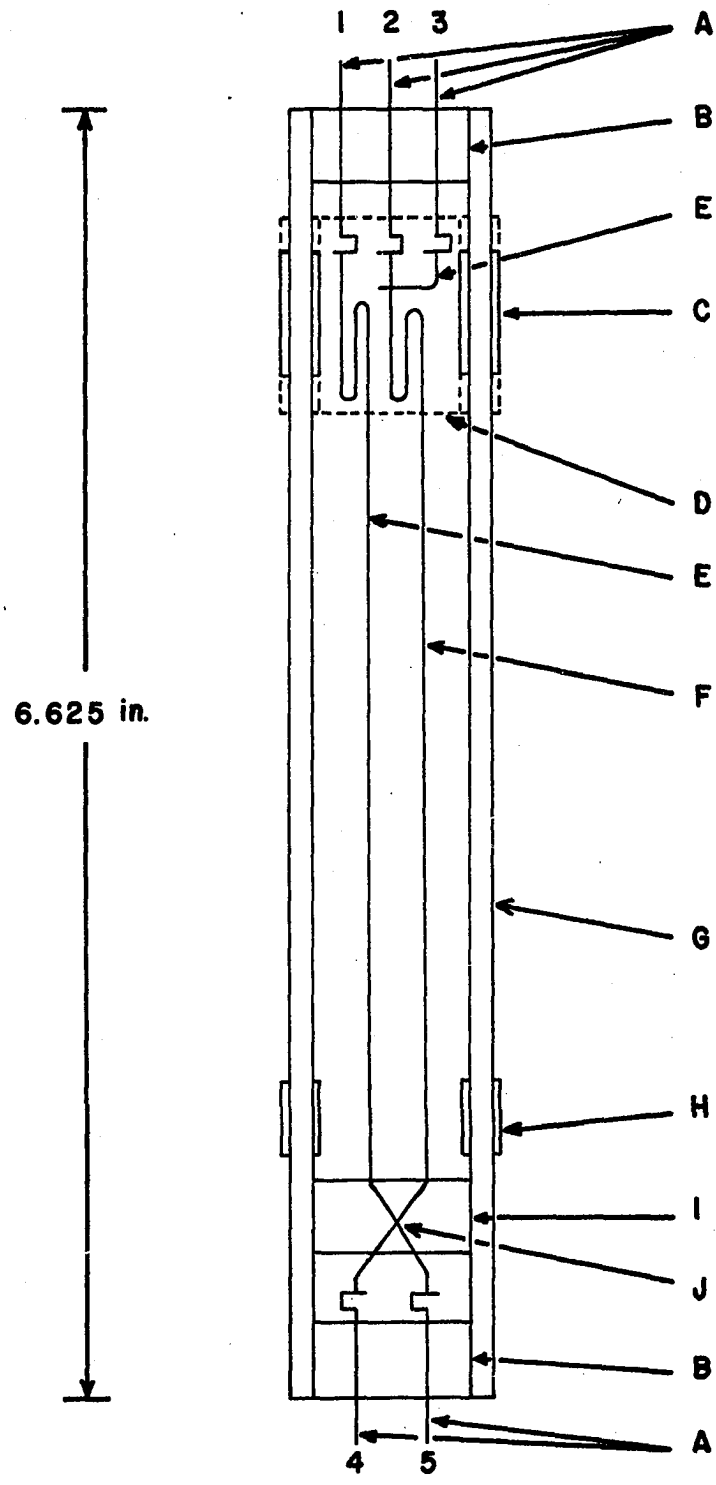
1.125 in.
1 2 3
A
B
E
C
D
E
F
G
H
I
J
B
A
4 5
6.625 in.

Figure 4. Heater Block.

A. Phenolic terminal mount.

B. Copper form.

C. Resistance thermometer cavity.

D. Resistance windings.

E. Hole for screw connection.

F. Stainless steel frame (cross section).

G. Position of sample hot junction.

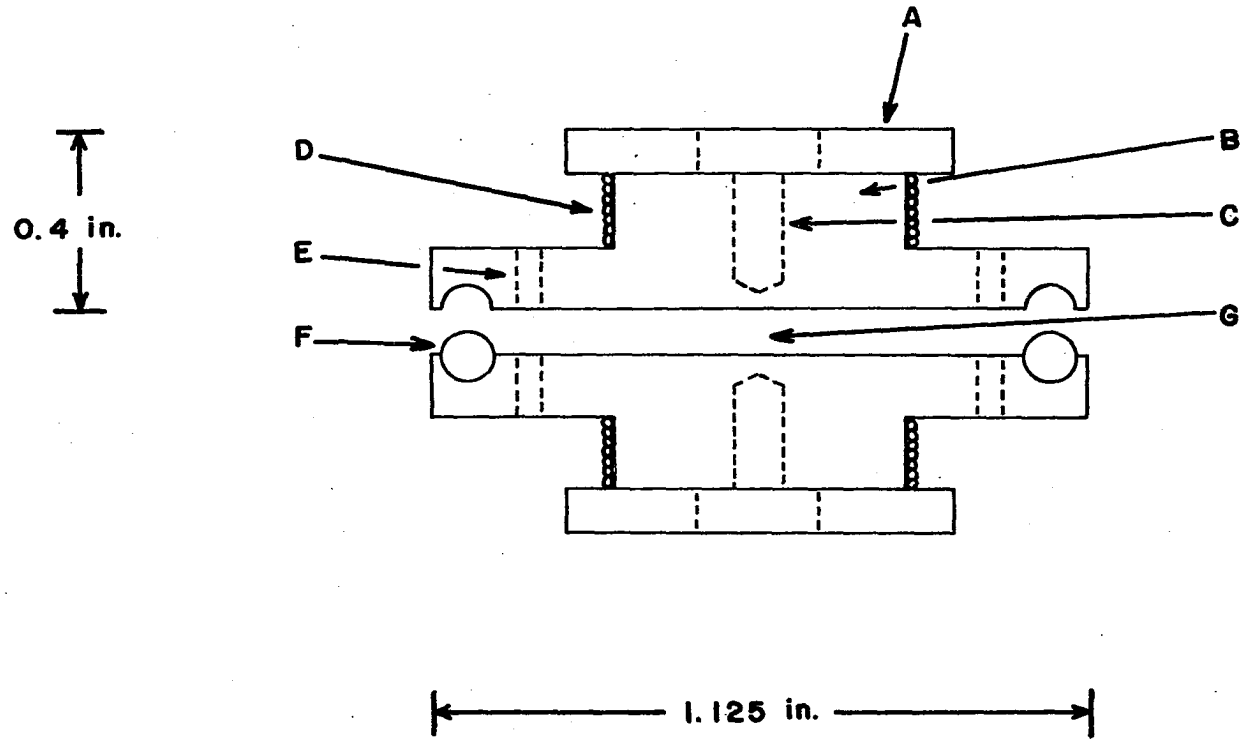
A
B
C
D
E
F
G
0.4 in.
1.125 in.

halves, which were then connected to each other by means of two small screws. Thermal linkage between the halves was achieved through these screws and through a liberal coating of silicone vacuum grease on the surfaces. The heater windings were made from Evanohm wire having an effective resistance of 100 Ω/ft. The windings were varnished to each half of the block with General Electric No. 7031 Adhesive and Insulating Varnish. The total resistance of the heater was 250 Ω.

In the center of each half of the heater block was a cavity to contain a resistance thermometer. Normally, a germanium resistance thermometer was placed in one side while a platinum thermometer was set in the other. Under this arrangement liquid helium and liquid nitrogen runs could be made back-to-back without demounting any of the apparatus. Phenolic terminal pieces were attached directly to the heater block so that the electrical connections leading to the outside of the cryostat would be located at a point where the temperature was essentially that of the heater block itself. Thus heat leaks along the thermometer leads themselves were minimized. Leads from the feedthroughs to the heater block were made of No. 34 enamelled copper magnet wire, the smallest diameter available at the time.

In a good vacuum the main source of heat leaks from the heater was thermal conduction along the sample, sample holder, and lead wires. The temperature controller initially in use could supply only a limited power (approximately 0.2 watt) to the heater; therefore, heat leak calculations like those in White's[16] book were carried out to determine a minimum distance between heater and thermal ground so that the entire temperature range between 4.2 K and 77 K could be spanned. However,

in actual practice this could not quite be achieved with that controller, nor could the temperature interval from 77 K to 300 K in liquid nitrogen be spanned. But a more powerful modification of the temperature controller worked very well with this sample holder.

E. Mounting the Sample

The sample consisted of a thermocouple. Generally one arm was made up of a 0.5 mm diameter wire of 69 pure indium while the other arm was a 0.5 mm diameter wire of a dilute alloy of indium. The mounting arrangement is depicted in Figure 3. The hot junction of the thermocouple was clamped between the two halves of the heater block at its center, and it was electrically insulated from the heater by a coating of General Electric No. 7031 varnish. The two arms of the thermocouple were cold welded together at the hot junction; for indium this is a very easy procedure. To obtain good thermal connection between the heater and the sample, silicone vacuum grease was applied to the parts.

The cold junction was made at the heat sink. Good thermal contact was insured by curling the sample as shown and by coating the parts with vacuum grease. A thin copper plate screwed onto the heat sink over the sample to hold it in place. Electrical insulation was achieved by coating the heat sink and its covering plate with varnish.

Another wire of 69 pure indium was cold welded to the alloy wire at the heat sink to provide a potential lead for determining resistance.

At the heat sink the sample wires were attached to copper

wires leading out of the cryostat. This connection was made by melting the sample wires directly onto the copper wires using a suitable flux.

F. Temperature Controller

Depicted in Figure 5 is a block diagram of the temperature controller, which is based on a design by Ries and Moore.[17] The sensing element was either a germanium resistance thermometer (in the liquid helium range) or a platinum resistance thermometer (in the liquid nitrogen range), both supplied by Scientific Instruments, Inc. of Lake Worth, Florida. For comparison a General Radio 1433-T precision decade resistor with range 0.00 to 1111.10 Ω was used. The sensing resistor was installed in a standard three-lead configuration. Typical excitation currents were 10-20 μamp.

The heart of the controller system was the bridge which compared the resistance of the sensor to the decade resistor. It utilized a toroidal transformer, which was wound by Western Electric in Oklahoma City. The off-balance A.C. voltage output from the secondary was fed first into a preamplifier, then into a phase sensitive detector.

The overall operation of the controller is depicted in the block diagram of Figure 5. Many of the separate circuits described by Ries and Moore were replaced with a PAR Model 124 Lock-In Amplifier manufactured by Princeton Applied Research Corporation of Princeton, New Jersey.

Also, the original controller circuit was modified after a design by Moreland and Tuma.[18] This was done in order to boost the maximum power output to the heater from 0.2 W to 2.5 W. This design

Figure 5. Block Diagram of Temperature Control Circuit.

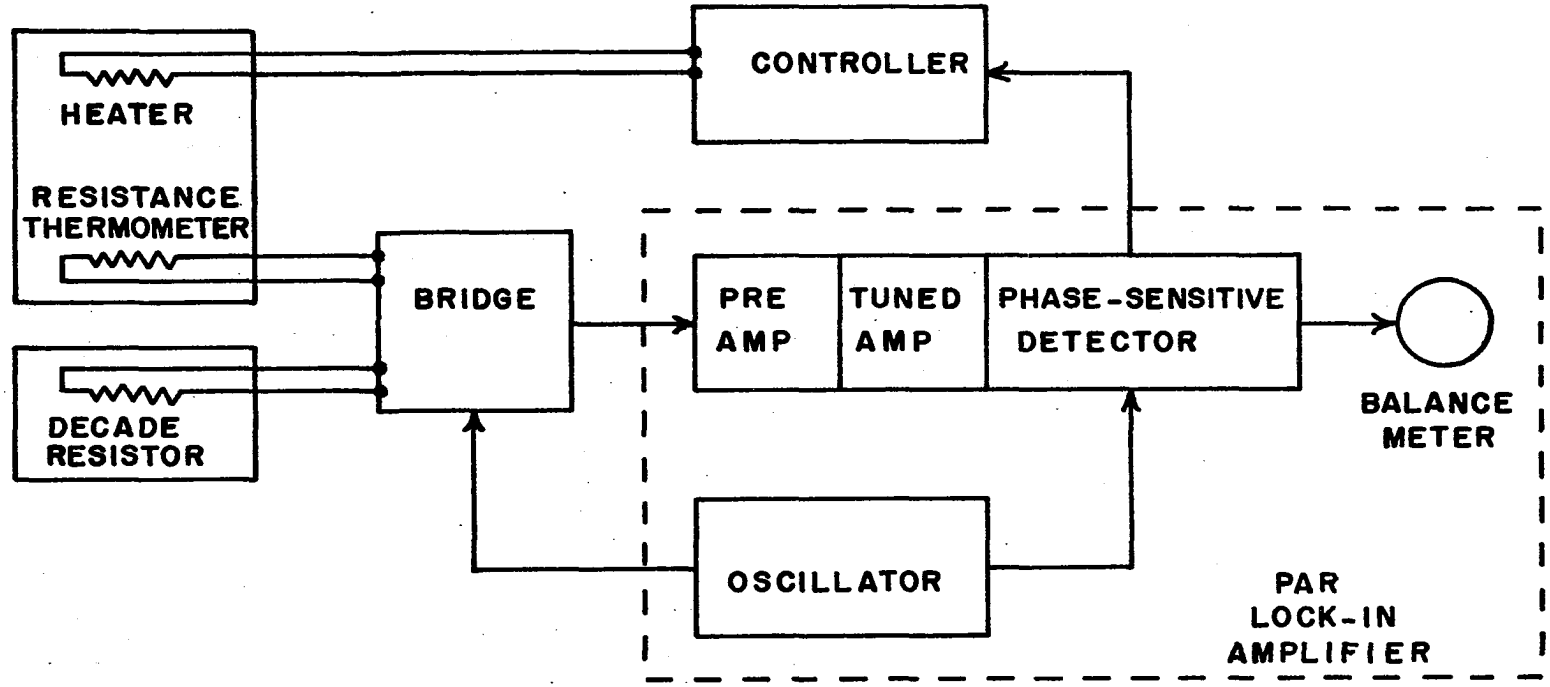
HEATER
RESISTANCE THERMOMETER
DECADE RESISTOR
CONTROLLER
BRIDGE
PRE AMP
TUNED AMP
PHASE-SENSITIVE DETECTOR
BALANCE METER
OSCILLATOR
PAR LOCK-IN AMPLIFIER

is shown in detail in Figure 6.

If reasonable care was observed in setting the controller circuits, control could be maintained to ± 0.0001 K at 4.2 K and ± 0.005 K at 77 K.

G. Calibration of the Germanium Resistance Thermometer

The germanium resistance thermometer was calibrated in the range 4.2 K to 100 K using a procedure similar to that described by Cataland and Plumb.[19]

Two germanium resistors calibrated by Scientific Instruments, Inc. were used in the calibration of the third uncalibrated resistor. One calibrated resistor was used as a sensor in controlling the temperature of a copper block which was wound with Evanohm heater wire having a total resistance of 250 Ω. All three resistances were placed in cavities in the block; vacuum grease was used to insure good thermal contact between the block and the resistors. The thermometer leads were collected at a phenolic terminal disc in thermal contact with the block itself. Heat leaks from the copper block to the liquid helium (or nitrogen) bath were along a 1/8 in stainless steel tube and various lead wires.

The unknown resistance was determined using a standard 4-lead technique. A schematic diagram of the calibration circuit is given in Figure 7. The direct current was determined by measuring the potential drop across a standard 10 ohm resistor, using a Leeds and Northrup K-4 potentiometer. Below 77 K the current was approximately 10 μamp; above it was approximately 100 μamp. The potential changes across the

Figure 6. Modified Controller Circuit of Moreland and Tuma (Reference 18).

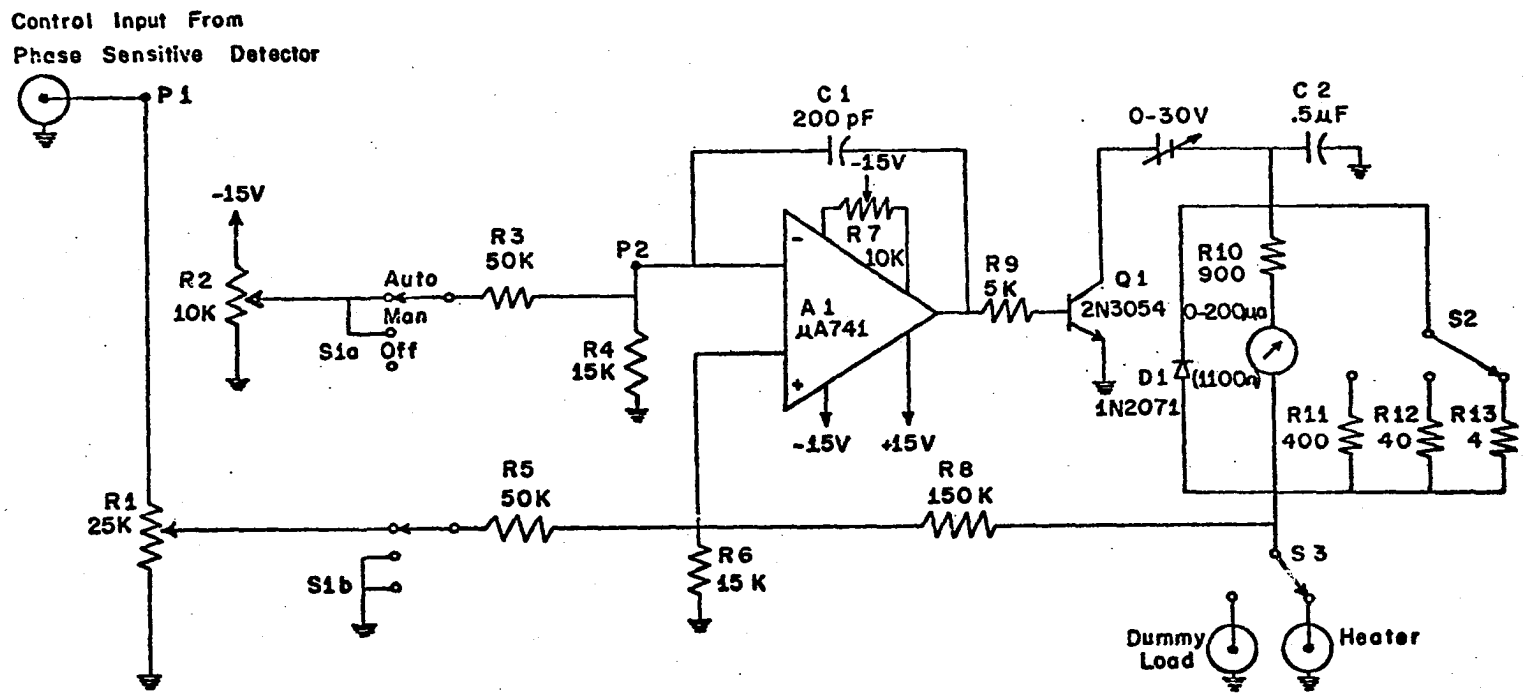
Control Input From
Phase Sensitive Detector
P1
-15V
R2
10K
Auto
Man
S1a Off
R3
50K
P2
R4
15K
C1
200 pF
-15V
R7
10K
A1
µA741
-15V
+15V
R9
5K
Q1
2N3054
D1
1N2071
0-30V
C2
.5µF
R10
900
0-200µa
(1100n)
S2
R11
400
R12
40
R13
4
R1
25K
R5
50K
S1b
R6
15 K
R8
150 K
S3
Dummy
Load
Heater

Figure 7. Block Diagram Calibration Circuit for the Germanium Resistance Thermometer.

R_1: Calibrated Resistance.

R_2: Uncalibrated Resistance.

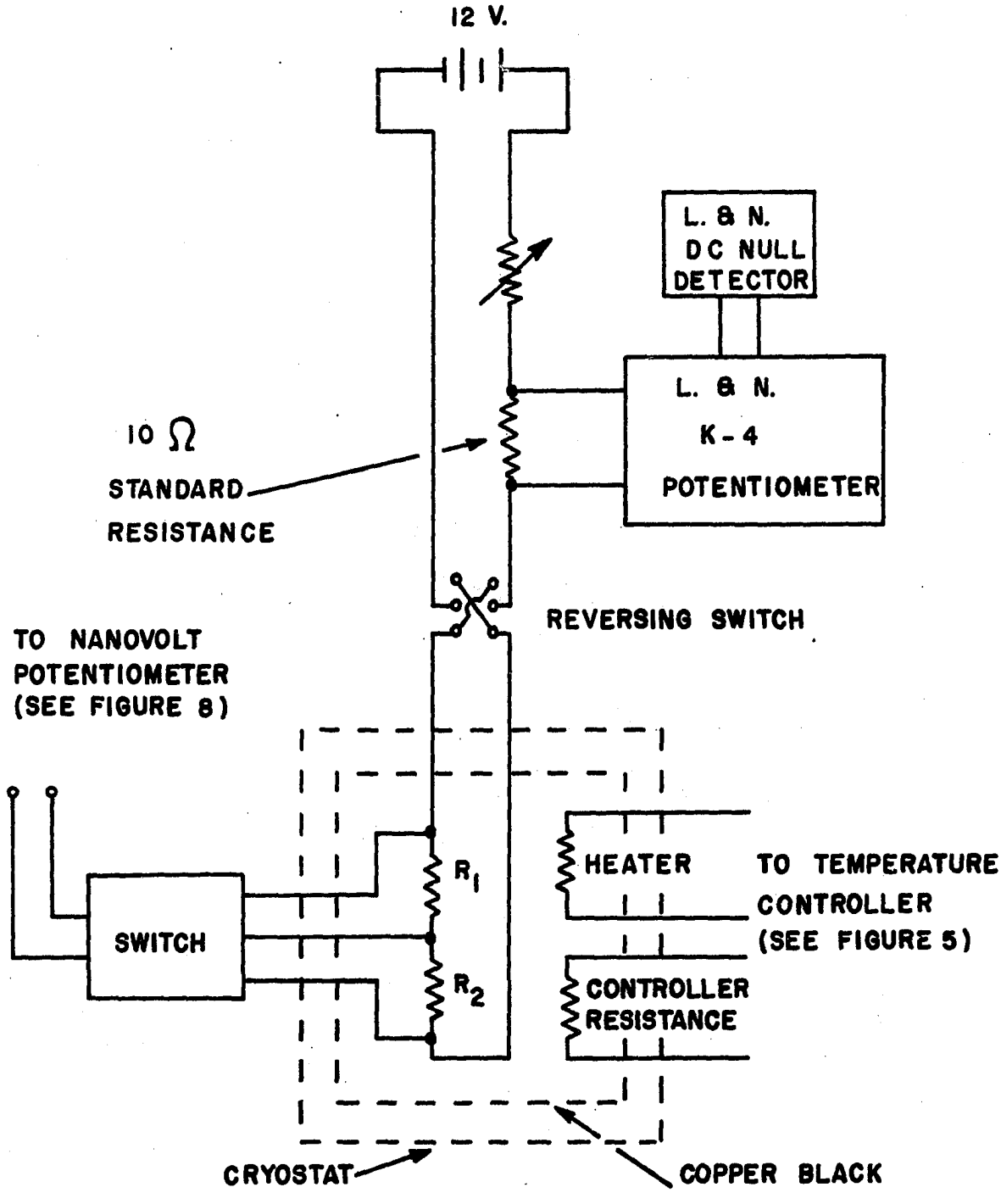
12 V.
L. & N.
DC NULL
DETECTOR
L. & N.
K-4
POTENTIOMETER
10 Ω
STANDARD
RESISTANCE
REVERSING SWITCH
TO NANOVOLT
POTENTIOMETER
(SEE FIGURE 8)
SWITCH
R1
R2
HEATER
TO TEMPERATURE
CONTROLLER
(SEE FIGURE 5)
CONTROLLER
RESISTANCE
CRYOSTAT
COPPER BLACK

known and unknown resistances, respectively, were measured with a Guildline Nanovolt Potentiometer.

At every calibration point the potentials across the known and unknown resistances, respectively, were measured twice with the current in the forward direction and twice with the current in the reverse direction. The reversing procedure takes into account the spurious thermoelectric potentials between the calibration block at low temperature and the potentiometer at room temperature. The resistance values calculated from each of these readings were averaged to give the resistance value at that point. The temperature intervals between successive points ranged from 0.25 K at 4.2 K to 5.0 K at 100 K.

No attempt was made to fit the data to a single function over the entire temperature range. Rather the unknown resistance R was determined as a function of temperature T by fitting the data, five points at a time, to the expression

$$R = Ae^{BT+CT^2}, \tag{3}$$

where A, B, and C are constants. The resistance was then obtained for the middle data point. By shifting the cluster of points one step at a time, the resistance of the thermometer as a function of temperature was obtained in tabular form over the entire range. Interpolations of the results were made to give the resistance at temperature intervals of 0.1 K.

The calibration was checked at the temperature of boiling nitrogen, with atmospheric pressure accounted for. The calibration yielded a temperature reading less than 0.02 K different from the known

temperature of boiling liquid nitrogen. A check was also made at the superconducting transition temperature of lead, which is 7.25 K. The calibration was easily within 0.05 K of the temperature and was probably even better. However, because this check was done in the course of obtaining thermoelectric data, no attempt was made to test the calibration more closely.

H. Sample Preparation

A few of the indium alloy samples used in this experiment were purchased in wire form directly from Cominco American, Inc. of Spokane, Washington. Some others were kindly provided by Dr. R. P. Huebener of the Argonne National Laboratory, but their ultimate source was Cominco American. However, most of the samples were alloyed and extruded at the University of Oklahoma, using a procedure similar to that described by Nicholson.[20]

For each dilute alloy that was prepared locally, the starting materials were 69 pure indium shot supplied by Cominco American and either 69 or 59 pure solute material. These materials and their sources are summarized in Table 2.

The alloying was done in a quartz tube of 6 mm I.D. In preparation for the mixing the tube was sealed at one end, then cleaned with aqua regia and rinsed with distilled water. It was necessary to deposit a light carbon film inside the tube to prevent adhesion of the molten metal to the quartz.

The indium was first etched in nitric or hydrochloric acid, melted in a quartz tube, degassed under vacuum, and etched again. A

Table 2. Alloy Components

Metal	Grade	Original Form	Source	Etch
In	69	Shot	Cominco	HNO_3 or HCl
Sn	69	Shot	Cominco	HNO_3
Pb	69	Wire	Cominco	
Cd	69	Ingot	Electronic Space Prod. Inc.	HNO_3
Ga	59	Rod	Electronic Space Prod. Inc.	None
Zn	69	Shot	Cominco	HNO_3

typical amount of indium used was 15 grams.

The solute was etched and weighed on a balance to the required amount to make a dilute alloy of 0.1 or 0.3 atomic percent impurity.

With the host and solute material in place the quartz tube was evacuated to approximately 0.01 torr and sealed under vacuum. The contents were melted and agitated in a flame for approximately one hour, then quenched into a water bath to keep the host and solute from separating. The resulting alloy slug was cut and etched in nitric acid in preparation for extrusion into wire. Alloys with higher concentration of the same impurity were prepared in the same manner using the existing alloy as a base.

The steel extrusion apparatus is described in detail by Nicholson.[20] The cylindrical alloy slug was contained in a cell and forced through a 0.5 mm die by a piston, to which pressure was applied via a hydraulic press. The resulting wire was then etched in nitric acid. The extrusion apparatus was cleaned between usages.

Pure indium wire was prepared in a similar manner. Resistance ratio [R(295 K)/R(4.2 K)] measurements made on the resulting samples compared favorably with measurements made on the commercially produced samples. In fact, some of the pure indium samples had slightly higher resistance ratios than the pure commercial samples. These results are summarized in Chapter IV.

Indium anneals readily at room temperature.[22] Tests were carried out on pure indium and dilute alloys containing thallium or tin to ascertain whether further annealing at 110°C affected the thermopower. No appreciable change in the thermopower of these samples

was observed. Therefore, in general the samples were allowed to anneal several days at room temperature before thermoelectric measurements were made.

I. Measurement Procedure

The procedure used for gathering data and determining the thermoelectric power as a function of temperature was similar to that described by Huebener.[14] The measurements were integral in nature, i.e., the thermal E.M.F. of the sample thermocouple was measured directly at succeeding temperatures of the hot junction. In liquid helium the range covered was 4.2 K to 100 K, while in liquid nitrogen it was 77 K to 350 K. Below 15 K the temperature interval was 0.5 K; it was generally 1.0 K between 15 K and 28 K, 2.0 K between 28 K and 50 K, 5.0 K between 50 K and 100 K, and 10.0 K above 100 K.

A block diagram of the E.M.F. measuring circuit is shown in Figure 8. It consisted of the following instruments (manufactured by Guildline Instruments, Ltd., Smith Falls, Ontario, Canada): Nanovolt Potentiometer Model 9176-G, Nanovolt Amplifier Model 9460A, Galvanometer Model 9461A.

The thermoelectric potential was measured across terminals 1 and 2 (or 3). (See Figure 3.) If terminal 1 (connected to pure indium) was labelled negative, the measured potential was that of the alloy referenced to the pure metal.

The temperature controller would be set to the desired temperature. When equilibrium had been achieved, the potential of the thermocouple was measured. In general changes in this potential could

Figure 8. Block Diagram of Circuit for Measuring Thermoelectric Potentials.

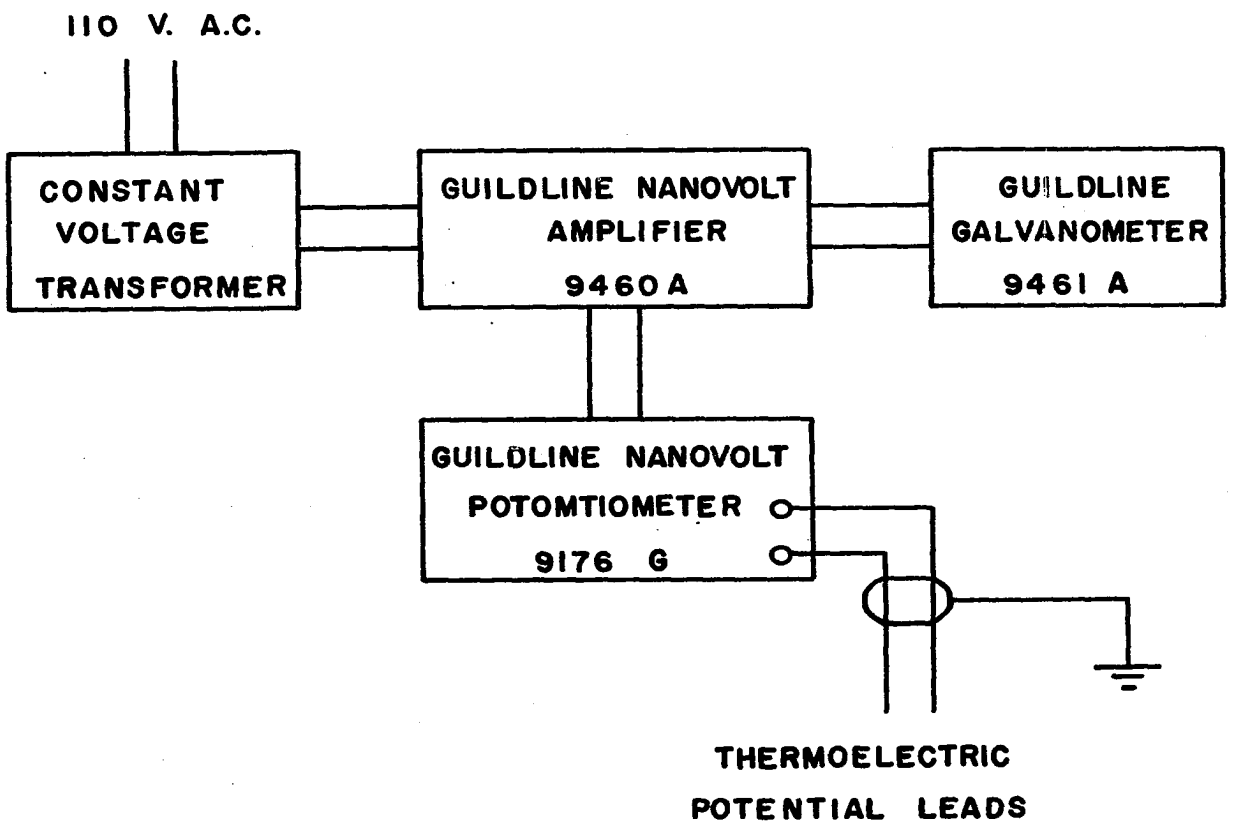
110 V. A.C.
CONSTANT VOLTAGE TRANSFORMER
GUILDLINE NANOVOLT AMPLIFIER 9460A
GUILDLINE GALVANOMETER 9461 A
GUILDLINE NANOVOLT POTOMTIOMETER 9176 G
THERMOELECTRIC POTENTIAL LEADS

be determined to ± 0.01 μV, and often a relative sensitivity of ± 0.005 μV was attained.

At each temperature the thermoelectric potential was measured once or twice. Sometimes, as an internal check, the potential was taken from terminals 1 and 3 (Figure 3) as well as 1 and 2. In liquid helium down-runs (100 K to 4.2 K) as well as up-runs were usually made. In liquid nitrogen only up-runs were made. Also the entire experiment was repeated for many of the alloys.

The up-runs in liquid helium were very reproducible for a given sample. However, there was often some small differences in the analyzed data of the down-runs. This may have been due to the fact that the heater block took much longer to reach equilibrium when going down the temperature scale. Only up-runs were used in the final analysis.

The data for each thermocouple was fit to a second-order polynomial by the method of least squares to give the thermal E.M.F. as a function of temperature. The entire curve was not fit to a single polynomial; rather, five, seven, or nine neighboring points were fit. Then the derivative was calculated for the center point. By shifting the cluster of neighboring points one step at a time, the difference in thermopower ΔS, where

$$\Delta S = S_{Alloy} - S_{Indium} \tag{4}$$

was obtained as a function of temperature. The seven point fits were used in all analyses.

The resistance of each dilute alloy sample was determined at 4.2 K and at 295 K by a standard 4-lead procedure. This is illustrated

in Figure 9. At each temperature two measurements of forward current and two of reverse current through the sample were made, using a Leeds & Northrup K-4 potentiometer. The corresponding potentials across the sample were measured using the Guildline Nanovolt Potentiometer. The resistance was determined for each set of readings, and the resulting values were used to calculate the average resistance of the specimen at each temperature.

Figure 9. Block Diagram of Circuit for Measuring the Resistance of the Sample.

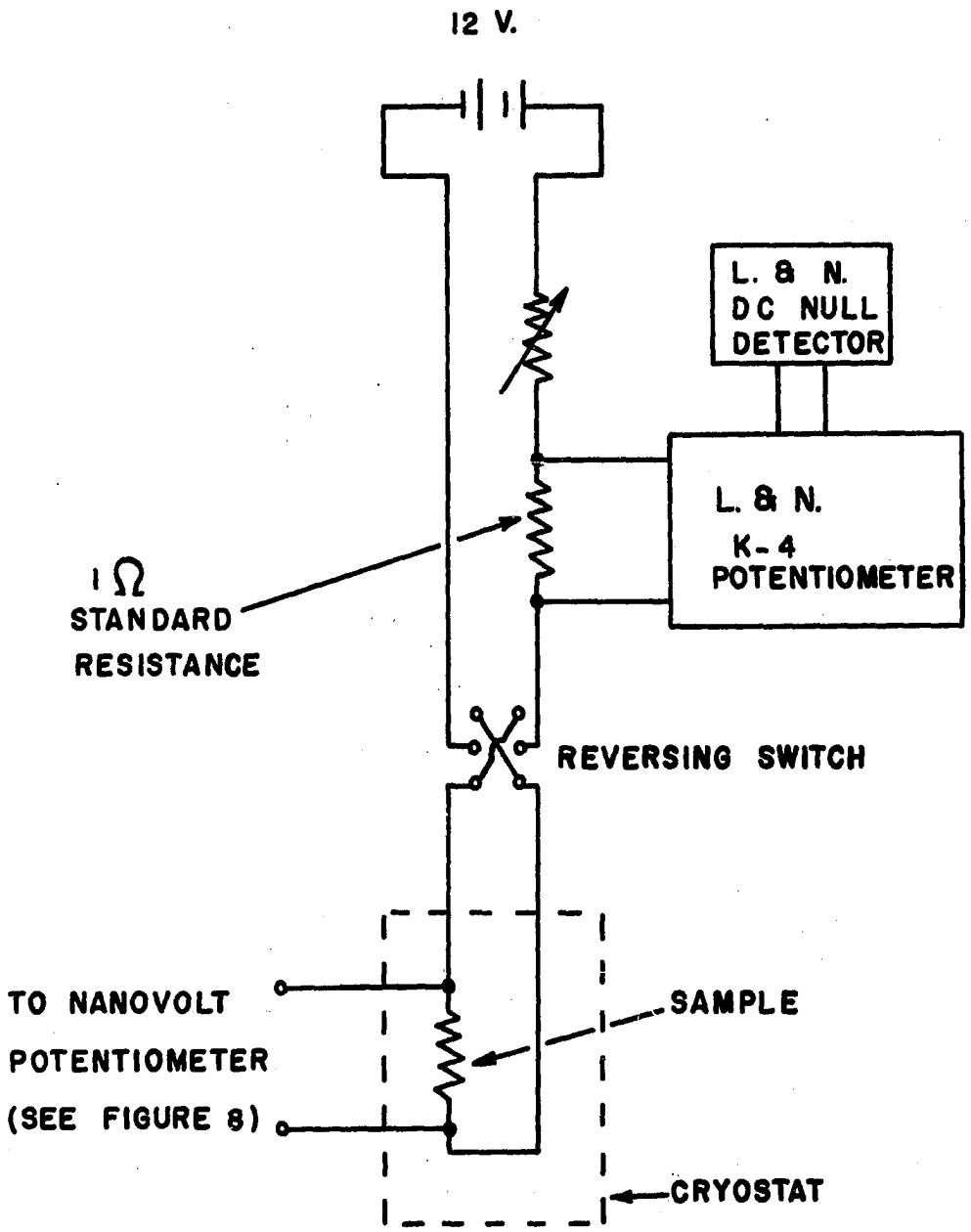
12 V.
L. & N.
DC NULL
DETECTOR
L. & N.
K-4
POTENTIOMETER
1 Ω
STANDARD
RESISTANCE
REVERSING SWITCH
TO NANOVOLT
POTENTIOMETER
(SEE FIGURE 8)
SAMPLE
CRYOSTAT

III. THEORETICAL DEVELOPMENT

A. Synopsis

It is assumed that the total thermopower S of a metal (in the pure or impure state) may be written

$$S = S_e + S_g, \tag{2}$$

where S_e is an electron (or hole) diffusion component and S_g is a phonon drag contribution. Theoretical expressions for these quantities are considered; in particular, the Nielsen-Taylor correction to S_e is discussed.

According to Equation (4) an initial analysis of the raw experimental data yields the difference ΔS between the total thermopower of the alloy and that of the pure metal. Therefore it is useful to consider the relation

$$\Delta S = \Delta S_e + \Delta S_g, \tag{5}$$

where ΔS_e and ΔS_g are, respectively, the change in the diffusion component and the change in the phonon drag component on alloying. Expressions for ΔS_e and ΔS_g as functions of temperature are obtained in order to fit the experimental data.

B. The Diffusion Thermopower

The diffusion thermopower may be conveniently written as the product of two terms:[9,22,23]

$$S_e = Q\xi, \tag{6}$$

where

$$Q = \frac{\pi^2 k_B^2 T}{3eE_F}, \tag{7}$$

and

$$\xi = \left[\frac{\partial \ln\sigma(\varepsilon)}{\partial \ln\varepsilon}\right]_{E_F} = -\left[\frac{\partial \ln\rho(\varepsilon)}{\partial \ln\varepsilon}\right]_{E_F} \tag{8}$$

where k_B is Boltzmann's constant, T is the absolute temperature, e is the charge (including sign) of the current carriers, $\sigma(\varepsilon)$ is the electrical conductivity, $\rho(\varepsilon)$ is the electrical resistivity, ε is the hypothetical energy of the Fermi level, and E_F is the actual Fermi energy.

Equation (6) was derived from the linearized Boltzmann equation under the assumption that the electron-phonon scattering processes regulating the electrical resistivity and the electronic thermal resistivity, respectively, are governed by the same relaxation time $\tau(\varepsilon)$. That is, the Wiedemann-Franz Law is assumed to hold.

Equation (6) is valid for energy ε any function of the electron wave number $\vec{k}$. It is valid for polyvalent metals as well as their alloys. Also it is valid for non-cubic as well as cubic crystal

symmetry. (For non-cubic single crystals S_e is a tensor quantity.)

Equation (6) gives the diffusion thermopower for a single conduction band. Real metals commonly have two conduction bands, and a similar equation could be written for each band. It is assumed here that a single band dominates the electrical conductivity and thermopower.

The dimensionless thermopower parameter ξ in Equation (8) is interpreted as follows. The Fermi energy ε is allowed to vary. The derivative of the conductivity $\sigma(\varepsilon)$ is then evaluated at the actual Fermi level E_F. Most treatments of ξ yield a result which is nearly independent of temperature T. Thus the diffusion thermopower is usually taken as a linear function of T. At very low temperatures deviations from the Wiedemann-Franz law are important. The effect of this is to decrease the value of ξ somewhat as $T \to 0$.[9]

C. Nielsen-Taylor Effect in Pure Metals

If a free electron model is adopted, then the thermopower parameter ξ of Equation (8) becomes[3,24]

$$\xi = \frac{3}{2} - \left[\frac{\partial \ln \frac{1}{\tau(\varepsilon)}}{\partial \ln \varepsilon}\right]_{E_F} \tag{9}$$

where $\tau(\varepsilon)$ is the assumed relaxation time governing electron-phonon interactions. From the linearized Boltzmann equation, the inverse relaxation time in terms of electron wave vector $\vec{k}$ is given by[4,23,25]

$$\frac{1}{\tau_{\vec{k}}} = \sum_{\vec{k}'} W(\vec{k},\vec{k}')\left(\frac{1-f_{\vec{k}'}}{1-f_{\vec{k}}}\right)\left[1 - \frac{\Lambda_{\vec{k}'}}{\Lambda_{\vec{k}}}\cos\theta_{\vec{k}\vec{k}'}\right]. \tag{10}$$

Here $W(\vec{k},\vec{k}')$ is the intrinsic probability for an electron to scatter from an occupied state $\vec{k}$ to an empty state $\vec{k}'$ via a phonon interaction. The probabilities that the states $\vec{k}$ and $\vec{k}'$ are occupied are given by $f_{\vec{k}}$ and $f_{\vec{k}'}$, respectively, the Fermi-Dirac distribution function. The electron-phonon mean free path is represented by Λ, and cubic symmetry is assumed in order to write this as a scalar. The angle between the initial and final wave vectors is $\theta_{\vec{k}\vec{k}'}$.

Nielsen and Taylor[3,4] calculate $\frac{1}{\tau_{\vec{k}}}$ and hence $\frac{1}{\tau(\varepsilon)}$ using a free electron model with $\varepsilon \propto k^2$. Then the thermopower parameter ξ is determined from Equation (9). The details of this derivation are complex and are not reproduced here. But a word of explanation on how this calculation differs from more standard methods is in order.

Normally, only first-order electron-phonon processes (Figure 10a) are taken into account when transport properties are calculated. Second-order processes involving virtual intermediate phonon states (Figure 10b) have generally been neglected on the basis of Migdal's Theorem.[26] This states that second-order contributions are on the order m/M smaller than the first order contribution, where m/M is the ratio of the electronic mass to the ionic mass. Nielsen and Taylor point out, however, that the contributions to the relaxation time of some second-order terms are highly energy dependent because they are proportional to the Fermi-Dirac function which is itself strongly energy dependent near the Fermi energy. Because the parameter ξ is dependent on the energy derivative of these terms, Nielsen and Taylor conclude that the second-order processes contribute significantly to the diffusion thermopower.

Figure 10. Typical Electron-Phonon Scattering (Reference 4).

(a) First order.

(b) Second order interactions of the type considered by Nielsen and Taylor.

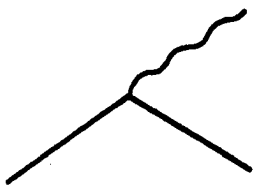

(a)

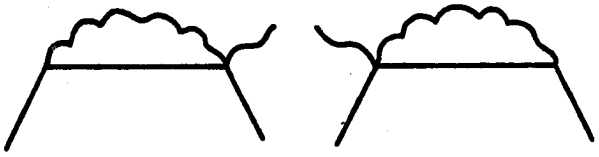

(b)

As a result of the Nielsen-Taylor calculations, ξ takes the form[4]

$$\xi = \xi_o + \Delta\xi_o \tag{11}$$

in a pure metal, where

$$\xi_o = 3-2\left[\frac{\partial \ln|V|}{\partial \ln\varepsilon}\right]_{E_F}, \tag{12}$$

and

$$\Delta\xi_o = \frac{E_F V}{k_B^2\theta^2}\frac{m}{M}\psi_1\left(\frac{T}{\theta}\right). \tag{13}$$

Here θ is the Debye temperature, V is the pseudopotential appropriate to the metal, and $\psi_1(\frac{T}{\theta})$ is a positive function which depends on valence as well as temperature. A graph of $\psi_1(\frac{T}{\theta})$ for valence 3 is given in Figure 11. The absolute value of its coefficient in Equation (13) is to order of magnitude unity.

The constant term ξ_o is identified as the thermopower parameter in the absence of second-order effects. It is commonly determined from experimental values of the diffusion thermopower via Equations (6) and (7) at high temperatures where phonon drag is negligible.

The term $\Delta\xi_o$ is associated with the second-order effects. It is inherently negative because of the attractive pseudopotential V. The value of V is discussed further in Chapter IV.

The absolute value of $\Delta\xi_o$, evaluated at the maximum value of $\psi_1(\frac{T}{\theta})$, is the Nielsen-Taylor figure of merit in Table 1. For use in

Figure 11. Graphs of the Functions $\psi_1(\frac{T}{\theta})$ (for valence 3), $\psi_2(\frac{T}{\theta})$, and $\psi_3(\frac{T}{\theta})$ (Reference 4).

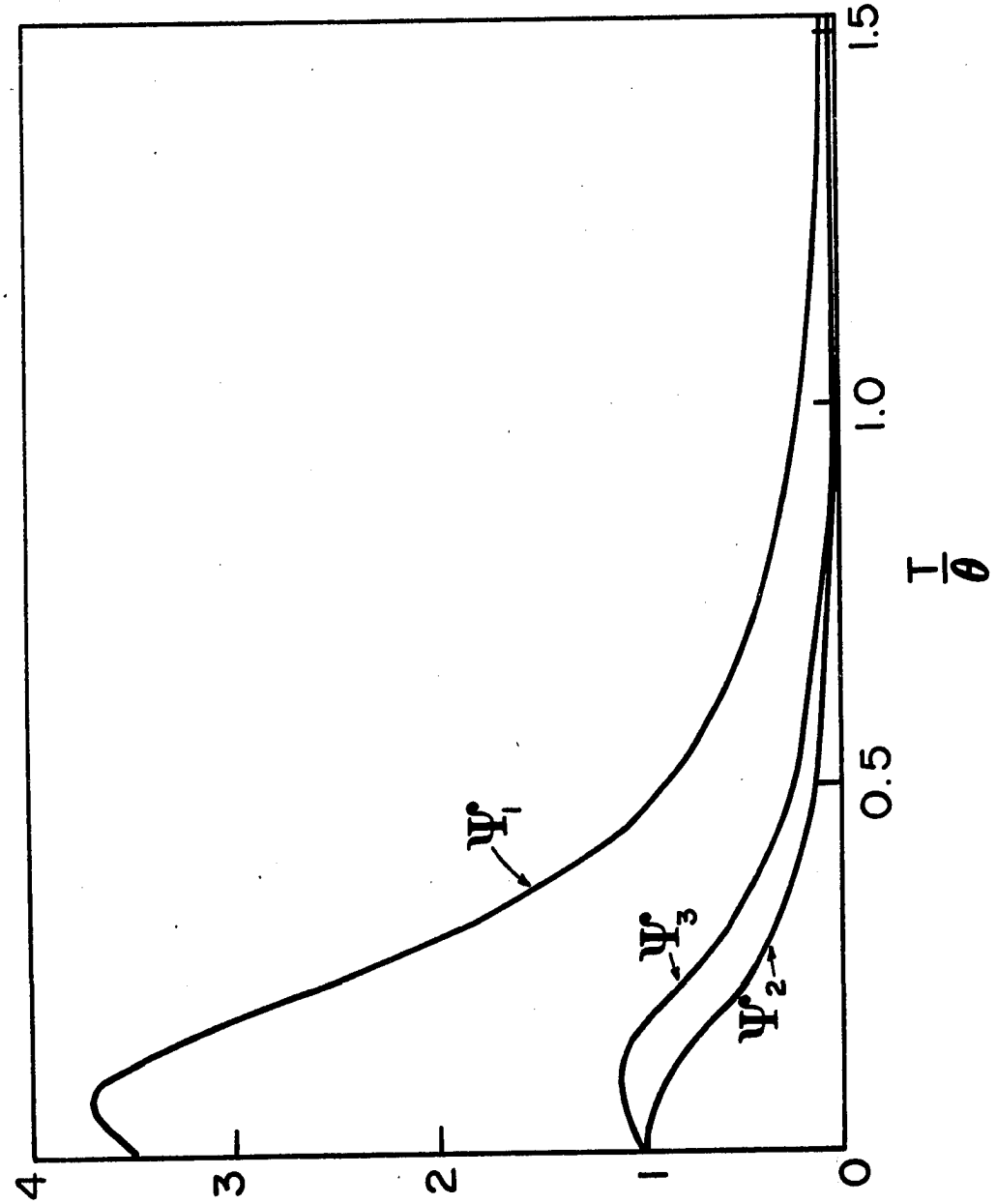
4
3
2
1
0
0.5
1.0
1.5
$\frac{T}{\theta}$
Ψ_1^*
Ψ_3^*
Ψ_2^*

this table the various constants for the different metals were taken from Harrison[27,28] and from The American Institute of Physics Handbook, Third Edition.[29] The specific heat effective electron mass was used in calculating the ionic to electron mass ratio M/m for each metal.

The behavior of $T\xi/\theta$, which is proportional to the thermopower, is given in Figure 12.[4] At high temperatures the thermopower is linear in T, as predicted by conventional theory. However, the minimum at approximately 0.1 T/θ is due to the correction term $\Delta\xi_o$.

D. The Effect of Impurities on the Diffusion Thermopower

In the determination of how the diffusion thermopower S_e changes if impurities (or other defects) are added to the pure metal, the following simplifying assumptions are made.[9]

(1) The Wiedemann-Franz Law holds. This must be true for Equation (8) to be valid.

(2) There is only one isotropic conduction band. Again, this must hold if Equation (6) by itself is to describe the diffusion thermopower.

(3) The heat transported by the charge carriers is independent of the heat transported by the lattice. In other words phonon drag effects are neglected.

(4) Matthiessen's rule holds. In other words all separate contributions to the total electrical resistivity ρ are independent of each other. This allows us to write

$$\rho = \rho_o + \rho_1 , \tag{14}$$

Figure 12. Form of $\xi T/\theta$ as a Function of the Reduced Temperature T/θ where $\xi = 1 - \frac{1}{2}\psi_1(\frac{T}{\theta})$ for a Monovalent Metal (Reference 4).

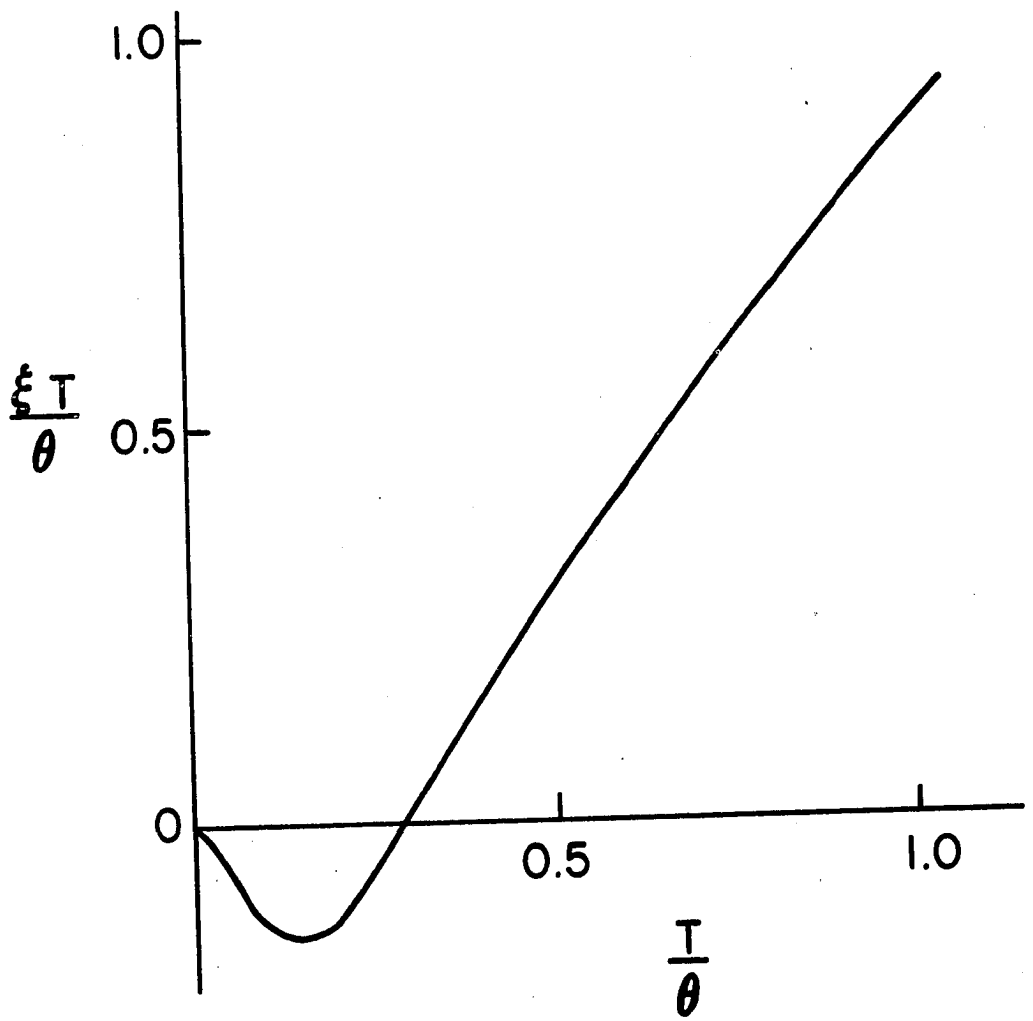
1.0
0.5
0
$\frac{\xi T}{\theta}$
0.5
1.0
$\frac{T}{\theta}$

where ρ_o is the resistivity as a function of temperature of the pure metal and ρ_1 is the additional resistivity due to the impurity.

Then inserting Equations (8) and (14) into Equation (6), we have

$$S_e = -Q\left[\frac{\partial \ln(\rho_o+\rho_1)}{\partial \ln \varepsilon}\right]_{E_F}, \tag{15}$$

where Q is the linear function of T defined by Equation (7). Here S_e is the resultant diffusion thermopower of the alloy. The logarithmic derivative is easily separable into terms identifiable with the diffusion thermopower of the pure metal and the characteristic diffusion thermopower of the impurity, respectively. If the logarithmic derivative is formally expanded, Equation (15) becomes

$$S_e = -QE_F\left[\frac{\rho_o}{\rho_o+\rho_1}\left(\frac{1}{\rho_o}\frac{\partial \rho_o}{\partial \varepsilon}\right) + \frac{\rho_1}{\rho_o+\rho_1}\left(\frac{1}{\rho_1}\frac{\partial \rho_1}{\partial \varepsilon}\right)\right]_{E_F}, \tag{16}$$

which is equivalent to

$$S_e = -\frac{\rho_o}{\rho_o+\rho_1} Q\left[\frac{\partial \ln \rho_o}{\partial \ln \varepsilon}\right]_{E_F} - \frac{\rho_1}{\rho_o+\rho_1} Q\left[\frac{\partial \ln \rho_1}{\partial \ln \varepsilon}\right]_{E_F}. \tag{17}$$

In the absence of second-order effects, the following identifications can be made:

$$\xi_o = -\left[\frac{\partial \ln \rho_o}{\partial \ln \varepsilon}\right]_{E_F}, \tag{18}$$

and

$$\xi_1 = -\left[\frac{\partial \ln \rho_1}{\partial \ln \epsilon}\right]_{E_F}. \tag{19}$$

These are the dimensionless thermopower parameters for the pure metal and the impurity, respectively. Then, analogous to Equations (6) and (8), we may write the total diffusion thermopower S_e of the alloy as

$$S_e = \frac{\rho_o}{\rho_o+\rho_1} S_{oe} + \frac{\rho_1}{\rho_o+\rho_1} S_{1e}, \tag{20}$$

where S_{oe} is the diffusion thermopower of the pure metal and S_{1e} is that of the impurity. This expression can also be derived in a different manner through a consideration of the pure metal and impurity constituents of the electronic thermal resistivity.[8,9]

At very low temperatures $\rho_1 >> \rho_o$, and hence the impurity dominates the thermopower in this region. At high temperatures $\rho_o >> \rho_1$, and the host dominates.

Most thermopower experiments are arranged to measure the thermopower difference ΔS between the alloy and the pure metal. The diffusion component is

$$\Delta S_e = S_e - S_{oe}, \tag{21}$$

which becomes

$$\Delta S_e = \frac{\rho_1}{\rho_o+\rho_1} (S_{1e} - S_{oe}). \tag{22}$$

In terms of ξ_o and ξ_1, this may be written

$$\Delta S_e = \frac{\rho_1}{\rho_o+\rho_1} S_{oe}\left[\frac{\xi_1}{\xi_o} - 1\right]. \qquad (23)$$

In standard analyses[9,30] Equation (23) is used to determine ΔS_e as a function of temperature. If second-order processes are not considered, then the expression in brackets is a constant. At high temperatures, the thermopower S_o is entirely diffusion in character, i.e., $S_o = S_{oe}$ and $\Delta S = \Delta S_e$. Both S_o and ΔS are known, experimentally determined quantities; thus the expression in brackets can be calculated at high temperatures. Also, ρ_o and ρ_1 are known. Then assuming S_{oe} to be linear in T, one can find ΔS_e as a function of temperature.

E. Nielsen-Taylor Theory for Alloys

The thermopower parameter for an impurity was written in Equation (19) as a constant ξ_1. This is the case when only first-order elastic scattering of carriers from the impurity ion is considered; this situation is illustrated in Figure 13a.

Nielsen and Taylor[4] considered the contributions of two types of virtual phonon states at the scattering site: one involving double scattering at the impurity, the other involving mixed scattering by the impurity and a phonon. These two types are illustrated in Figures 13b and 13c, respectively.

It was found that each type of scattering contributed an additive, temperature dependent correction to the impurity thermopower parameter. These corrections are, respectively,[4]

Figure 13. Typical Electron-Impurity Scattering (Reference 4).

(a) First order.

(b) Double scattering at an impurity site with second order virtual phonon.

(c) Single scattering at an impurity site with second order virtual phonon.

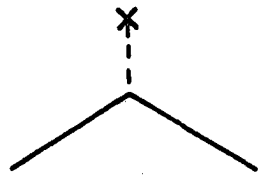

(a)

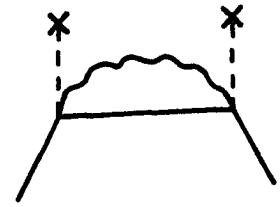

(b)

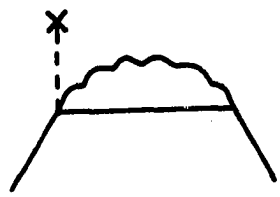

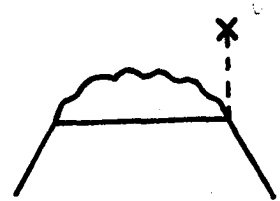

(c)

$$\Delta\xi_B = 6 \frac{E_F U}{(k_B\theta)^2} \frac{m}{M} \frac{N'}{N} \psi_2(\frac{T}{\theta}), \tag{24}$$

and

$$\Delta\xi_C = \frac{E_F V}{(k_B\theta)^2} \frac{m}{M} (\frac{2N}{N'})^{1/3} \psi_3(\frac{T}{\theta}), \tag{25}$$

where N'/N is the valence of the host and U is some "effective" pseudopotential difference between host and the impurity. A discussion of U is delayed until Chapter IV. The dimensionless functions $\psi_2(\frac{T}{\theta})$ and $\psi_3(\frac{T}{\theta})$, shown in Figure 11, become small for $T \gtrsim \theta$. The first-order constant ξ_1 was also determined:[4]

$$\xi_1 = \frac{5}{2} - 2[\frac{\partial \ln|U|}{\partial \ln\varepsilon}]_{E_F}. \tag{26}$$

The total thermopower parameter for the impurity is then the sum $\xi_1 + \Delta\xi_B + \Delta\xi_C$.

While $\Delta\xi_C$ is inherently negative because of the attractive potential V, the term $\Delta\xi_B$ may conceivably be positive or negative depending on the particular solute. All the terms will be discussed in more detail in Chapter IV.

Putting the results of this section and Equation (11) into Equation (17), we have

$$\Delta S_e = \frac{\rho_1}{\rho_o+\rho_1} Q[\xi_1+\Delta\xi_B+\Delta\xi_C-\xi_o-\Delta\xi_o], \tag{27}$$

the expected change in the diffusion thermopower on alloying, including

the Nielsen-Taylor corrections.

F. Phonon Drag Thermopower in Pure Metals

Equation (6) was derived under the assumption that the phonon distribution of the crystal lattice is in thermal equilibrium. The phonon drag contribution S_g to the thermopower arises from the net force which the non-equilibrium phonon flux of the lattice may exert on the conduction electrons.[9]

A simple consideration of the electron-phonon interaction shows that there should be two types of phonon drag. Figure 14a illustrates the "normal" scattering on a free electron Fermi surface of an electron of wave vector $\vec{k}$ by a phonon of wave vector $\vec{q}$ resulting in an electron of wave vector $\vec{k}'$. Momentum is conserved in this process, so we have

$$\vec{k}' = \vec{k} + \vec{q}. \tag{28}$$

If the entire phonon distribution is summed over, there is a net effect on the electron distribution in the direction of the phonon drift. Figure 14b illustrates an electron-phonon scattering process which includes a Bragg reflection in the crystal lattice. Electron-phonon momentum is not conserved in this process, and we have

$$\vec{k}' = \vec{k} + \vec{q} + \vec{g}\ , \tag{29}$$

where $\vec{g}$ is a reciprocal lattice vector. The net effect on the electron distribution from this "Umklapp" scattering is in a direction opposite to that of the net phonon drift.

In summary one can predict that, if the dominant charge carriers

Figure 14. Electron-Phonon Scattering on a Free Electron Fermi Surface. F. S., Fermi Surface; B. Z., Brillouin Zone.

(a) Normal process.

(b) Umklapp process.

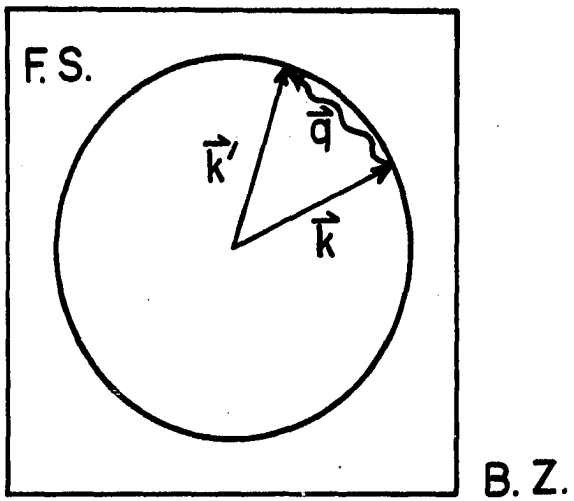

(a)

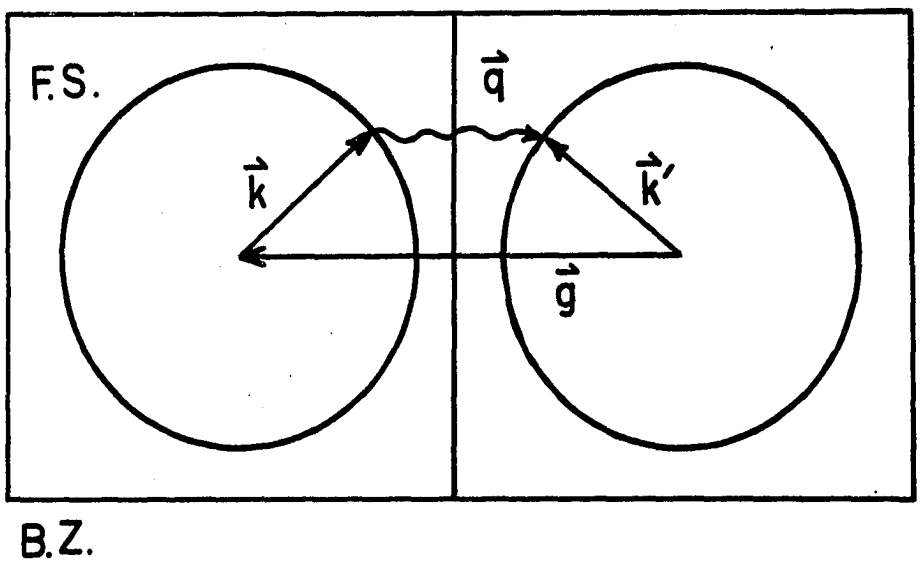

(b)

in the metal are electrons, the normal phonon drag thermopower should be negative and the Umklapp thermopower should be positive. Just the reverse is expected if the charge carriers are positive.[9]

Bailyn[31] and MacDonald[8] have argued that the phonon drag contribution to the thermopower should be of the form

$$S_g \sim \left(\frac{C_g}{ne}\right)\alpha, \tag{30}$$

where C_g is the lattice specific heat per unit volume, n is the number of charge carriers per unit volume, and α is the relative probability of a phonon to interact with an electron in comparison with all the other things (imperfections, other phonons) it may interact with.

At very low temperatures $T<<\theta$, the phonon-electron interaction dominates in a pure metal, i.e., $\alpha\sim 1$, while $C_g \sim T^3$. At high temperatures $T>>\theta$, $C_g \sim$ constant while $\alpha \sim T^{-1}$ due to the fact that phonon-phonon interaction dominate in this region. Thus, one expects

$$\begin{aligned} S_g &\sim T^3, \qquad T << \theta; \\ S_g &\sim T^{-1}, \qquad T >> \theta. \end{aligned} \tag{31}$$

A plot of this idealized phonon drag thermopower S_g is shown in Figure 15, along with the idealized component S_e.

Typically in real metals the phonon drag peak occurs at approximately $\theta/5$. Below this peak one might hope to fit the total thermopower S to the equation

$$S = AT + BT^3, \tag{32}$$

Figure 15. Idealized Thermopower of a Metal with Hole-Like Charge Carriers.

A. Diffusion Component.

B. Phonon Drag Component.

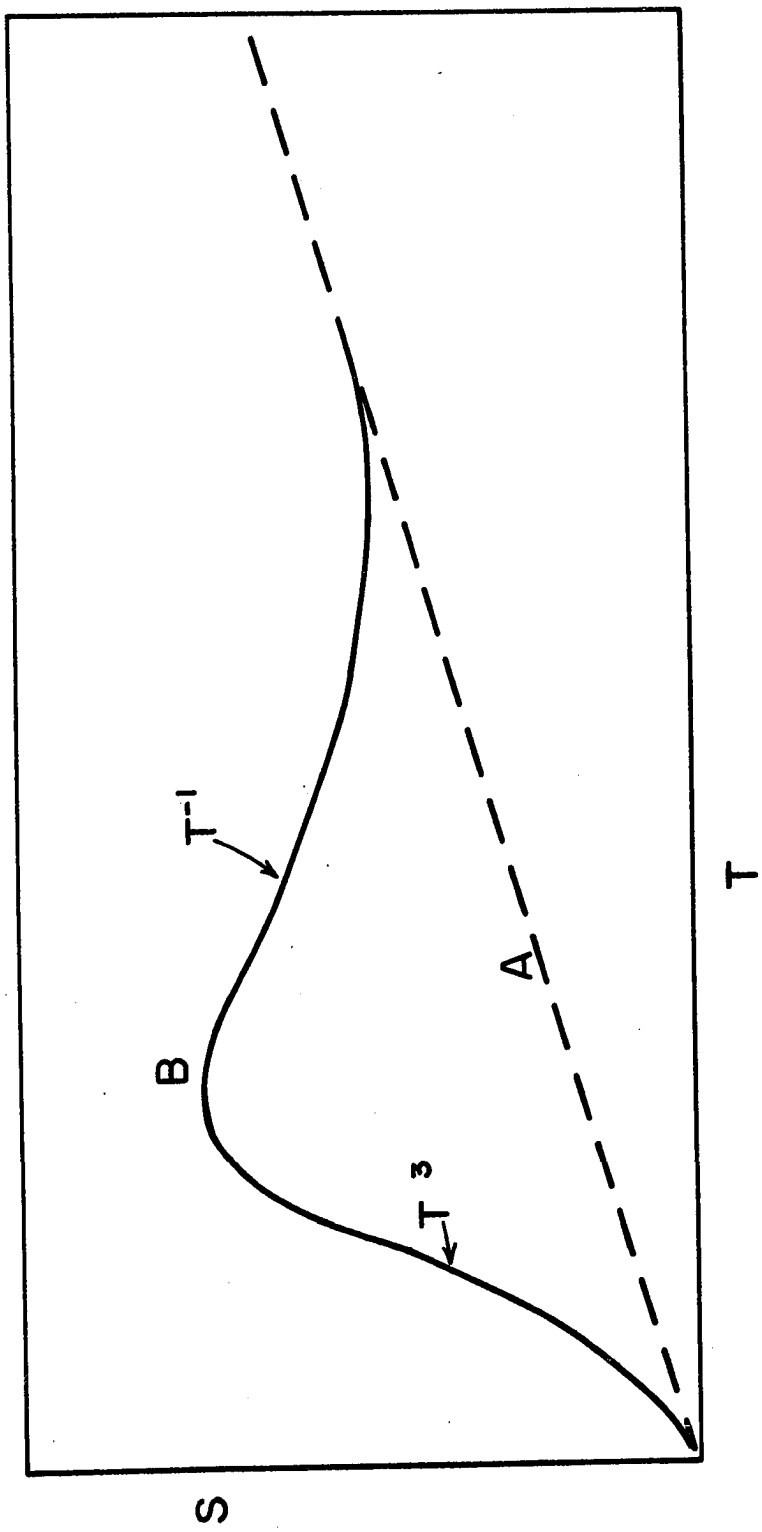
S
T
A
B
T^{-1}
T^{3}

where A and B are constants. Such fits have been made by Gold et. al.[32] for lead and by De Vroomen et. al.[33] for aluminum. The results are convincing only over a very narrow temperature range below 10 K where the approximation $\alpha \sim l$ is still reasonably valid.

Using the Debye approximation and neglecting dispersion of the phonon spectrum, Hanna and Sondheimer[34] have derived the following expression for pure metal phonon drag thermopower S_{og} due to normal processes:

$$S_{og} = A\left(\frac{T}{\theta}\right)^3 \int_0^{\frac{\theta}{T}} D(z)\alpha_o(z)dz, \tag{33}$$

where A is a constant, and

$$D(z) = \frac{z^4 e^z}{(e^z-1)^2}, \tag{34}$$

the Debye integrand. Here $z = \frac{\hbar\omega}{k_B T}$, where $\hbar$ is Planck's constant divided by 2π, and ω is the phonon frequency. The relative probability $\alpha_o(z)$ for an electron-phonon interaction in a pure metal is written as an implicit function of ω. Huebener[35] has shown that Equation (33) may be applied to the thermopower due to Umklapp processes also.

In a pure metal $\alpha_o(z)$ takes the form

$$\alpha_o(z) = \frac{\frac{1}{\tau_{pe}(z)}}{\frac{1}{\tau_o(z)}}, \tag{35}$$

where

$$\frac{1}{\tau_o(z)} = \frac{1}{\tau_{pe}(z)} + \frac{1}{\tau_{pp}(z)} \cdot \tag{35}$$

Here $\tau_{pe}(z)$ and $\tau_{pp}(z)$ are the relaxation times for electron-phonon processes and phonon-phonon processes, respectively. The total relaxation time for phonon scattering in the pure metal is $\tau_o(z)$.

G. The Effect of Impurities on the Phonon Drag Thermopower

An impurity introduced into a pure metal represents an additional scattering center for phonons. The effect of this is to reduce the number of phonons available for electron-phonon scattering. The relative probability $\alpha(z)$ for this scattering may then be written:

$$\alpha(z) = \frac{\frac{1}{\tau_{pe}(z)}}{\frac{1}{\tau_{pe}(z)} + \frac{1}{\tau_{pp}(z)} + \frac{1}{\tau_1(z)}}, \tag{37}$$

where τ_1 is the relaxation time for phonon-impurity interactions.

Analogous to Equation (33), the phonon drag thermopower S_g for a dilute alloy becomes

$$S_g = A\left(\frac{T}{\theta}\right)^3 \int_o^{\frac{\theta}{T}} D(z)\alpha(z)dz. \tag{38}$$

The expected effect of $\alpha(z)$ is to reduce S_g from its value in the pure metal. This change ΔS_g is defined as

$$\Delta S_g = S_g - S_{og}. \tag{39}$$

Putting Equations (33), (35), (36), (37), and (38) into Equation (39), and simplifying, one obtains the result

$$\Delta S_g = -A\left(\frac{T}{\theta}\right)^3 \int_0^{\frac{\theta}{T}} \frac{D(z)\alpha_o(z)dz}{1 + \frac{\tau_1(z)}{\tau_o(z)}}. \qquad (40)$$

Equation (40) is difficult to evaluate, chiefly because of the unknown behavior of the relaxation times involved. Certain simplifying assumptions can be made, however, and these will be discussed in Chapter IV.

IV. RESULTS AND ANALYSIS

A. Experimental Results

The pure indium and dilute alloy specimens used in the experiment are summarized in Table 3, along with the source, resistance ratio R(295 K)/R (4.2 K), and residual resistivity ρ_1 of each alloy. The residual resistivity of each alloy was calculated from the resistance at 4.2 K and the physical dimensions of the specimen.

A graph of the thermopower S of indium as a function of temperature is given in Figure 16. The values of S were obtained using a method similar to that described in Chapter II, Section I. A wire of 69 grade lead was used as the thermoelectric reference. The thermopower of lead as a function of temperature has been tabulated by Christian et. al.[36] These values were added to the experimentally obtained thermopower $\Delta S_{In,Pb}$ of the indium-lead thermocouple to yield the thermopower of indium as a function of temperature.

The peak at 21 K is assumed to be due to phonon drag. Then the phonon drag thermopower S_g is obtained by subtracting the full Nielsen-Taylor curve from the experimental curve.

Graphs for the measured change ΔS in the thermopower on alloying as a function of temperature are given for the various alloys as the dotted line in Figures 17-29. These were obtained using the pro-

Table 3. Composition of the Specimens

Nominal Impurity	Extrusion	$\frac{R(295\ K)}{R(4.2\ K)}$	ρ_1 ($10^{-8}\ \Omega$ cm)	Figure No.
pure	A	9720	0.09*	16
pure	B	10920	0.08*	16
0.1 at. % Tl	A	441	2.12	17
0.3 at. % Tl	A	151	7.63	18
0.1 at. % Sn	B	231	3.74	19
0.2 at. % Sn	B	112	8.23	20
0.3 at. % Sn	A	53	17.0	21
0.1 at. % Cd	B	240	3.36	22
0.3 at. % Cd	A	79	11.2	23
0.1 at. % Pb	B	154	5.65	24
0.3 at. % Pb	A	51	17.3	25
0.1 at. % Ga	B	559	1.49	26
0.3 at. % Ga	B	204	4.24	27
0.3 at. % Mg	A	165	6.40	28
0.1 at. % Zn	B	3920	0.25	29

A: Extruded by Cominco American, Inc.

B: Extruded by the author from material supplied by Cominco.

* Value of ρ_o at 4.2 K.

Figure 16. Thermopower of 69 Grade Polycrystalline Indium as a Function of Temperature.

Full curve: Composite of total thermopower of first two samples of Table 3.

Dashed curve: Assumed first order diffusion component.

Dotted curve: Diffusion component with Nielsen-Taylor corrections.

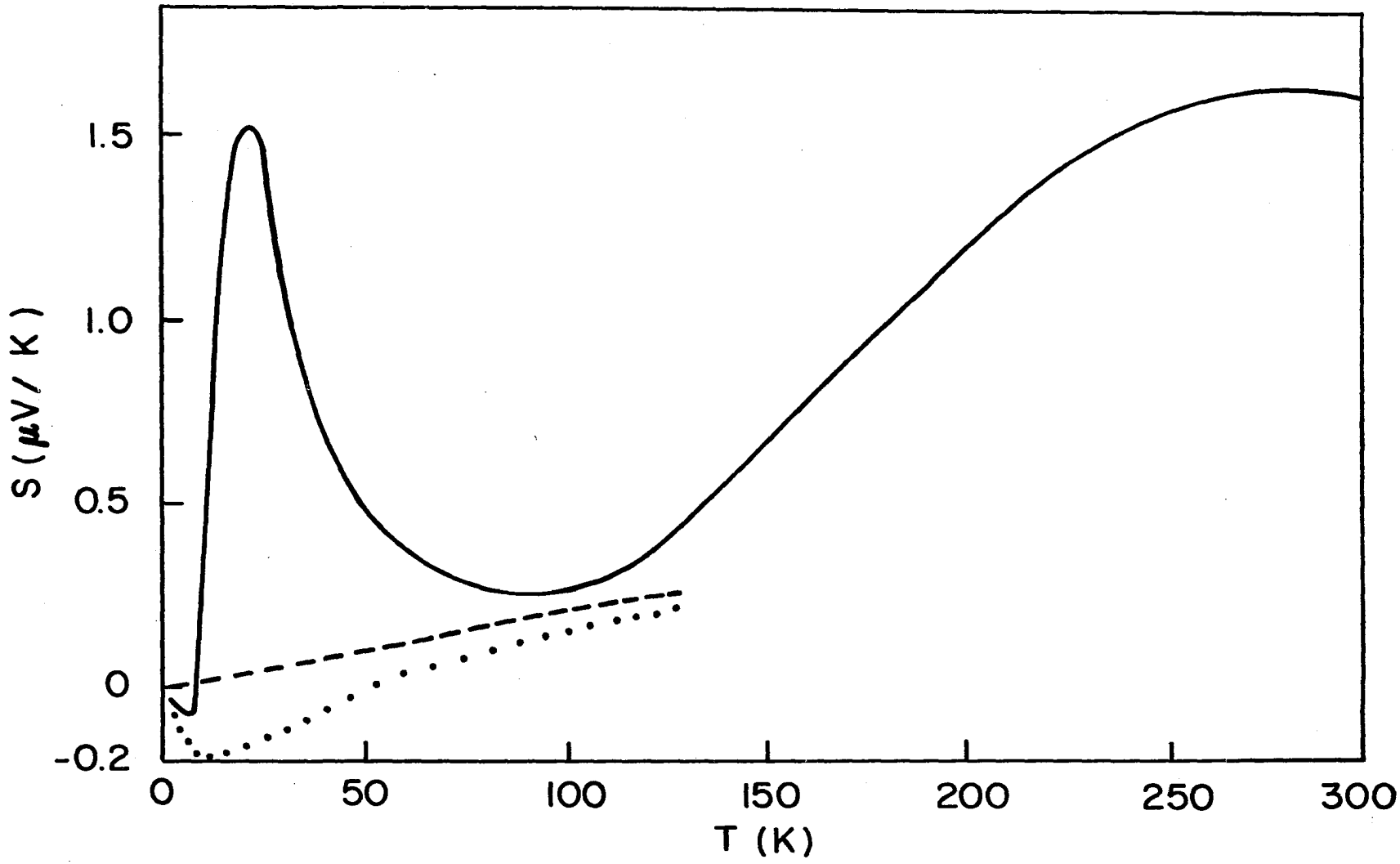
1.5
1.0
0.5
0
-0.2
S (μV / K)
0
50
100
150
200
250
300
T (K)

Figure 17. Thermopower of the Alloy In + 0.1 At. % Tl vs Pure Indium.

●—● Measured data ΔS.

1. Calculated Nielsen-Taylor effect ΔS_e.
2. Calculated phonon drag effect ΔS_g.

—— Calculated total thermopower change: 1 + 2.

(unlabelled)

3. Calculated diffusion thermopower without Nielsen-Taylor effect.

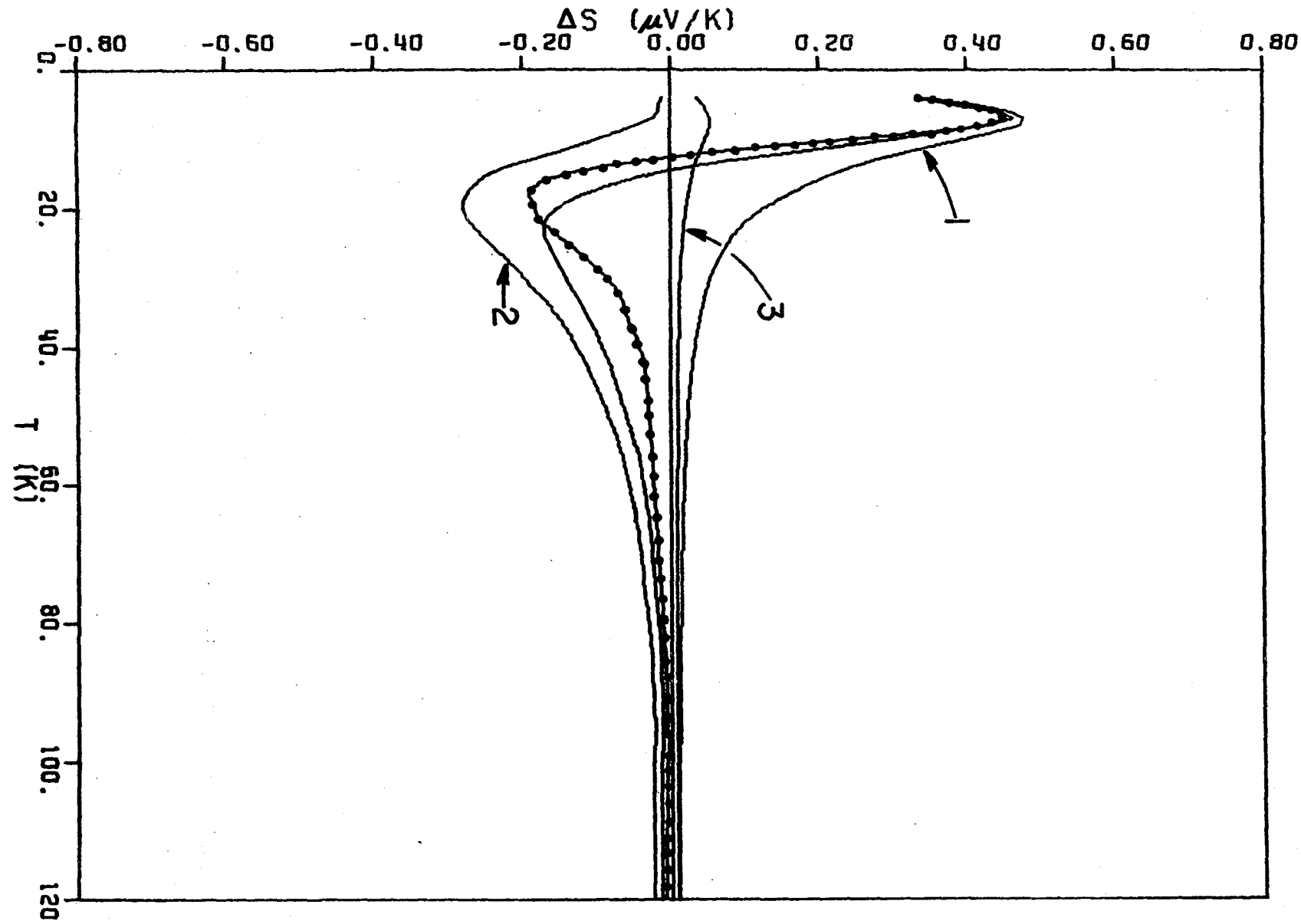
ΔS (μV/K)
-0.80
-0.60
-0.40
-0.20
0.00
0.20
0.40
0.60
0.80
0.
20.
40.
60.
80.
100.
120
T (K)
1
2
3

Figure 18. Thermopower of the Alloy In + 0.3 At. % Tl vs Pure Indium.

•—• Measured data ΔS.

1. Calculated Nielsen-Taylor effect ΔS_e.
2. Calculated phonon drag effect ΔS_g.

—— Calculated total thermopower change: 1 + 2. (unlabelled)

3. Calculated diffusion thermopower without Nielsen-Taylor effect.

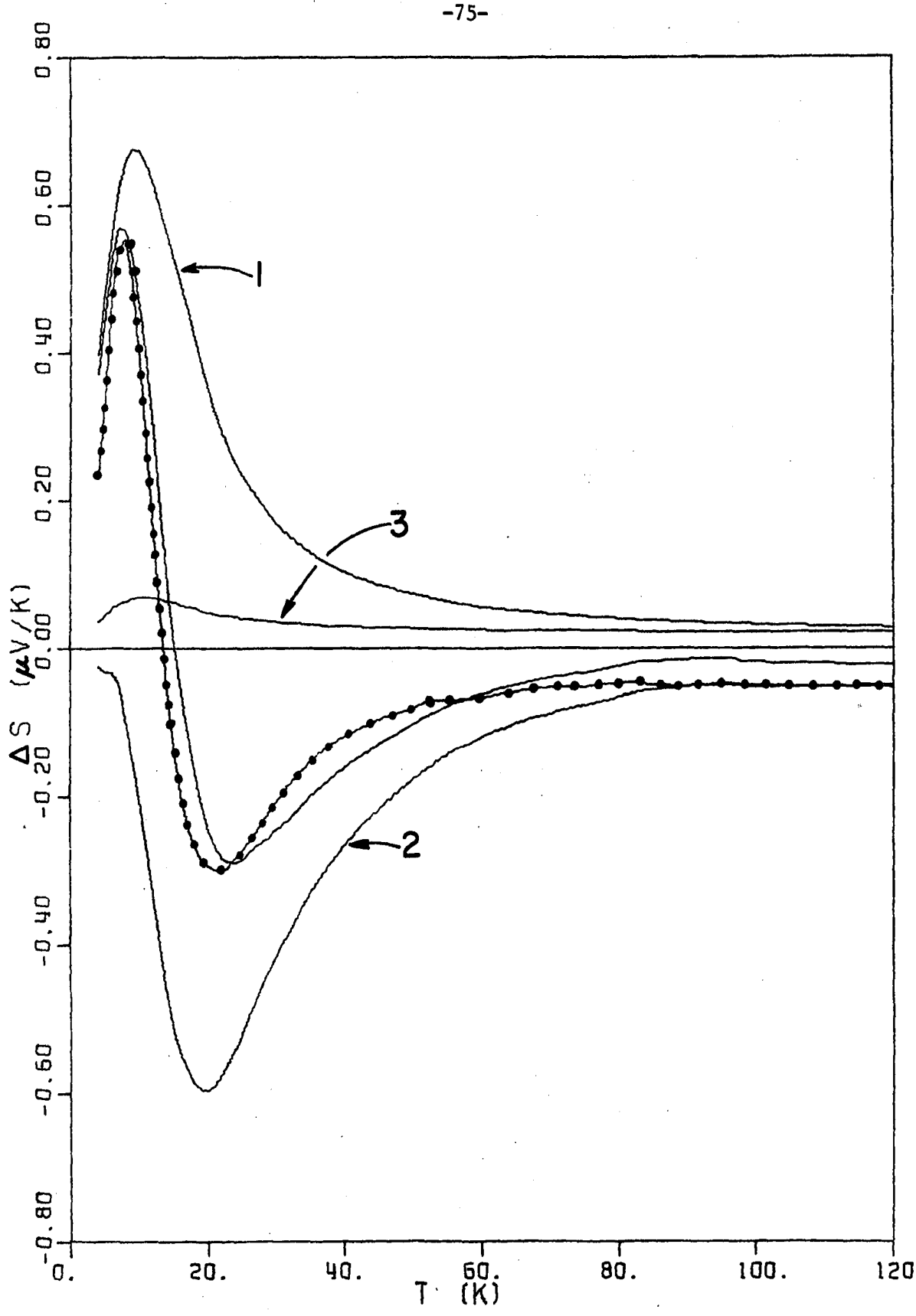
0.80
0.60
0.40
0.20
0.00
-0.20
-0.40
-0.60
-0.80
ΔS (μV/K)
0.
20.
40.
60.
80.
100.
120
T (K)
1
2
3

Figure 19. Thermopower of the Alloy In + 0.1 At. % Sn vs Pure Indium.

-●-● Measured data ΔS.

1. Calculated Nielsen-Taylor effect ΔS_e.

2. Calculated phonon drag effect ΔS_g.

—— Calculated total thermopower change: 1 + 2. (unlabelled)

3. Calculated diffusion thermopower without Nielsen-Taylor effect.

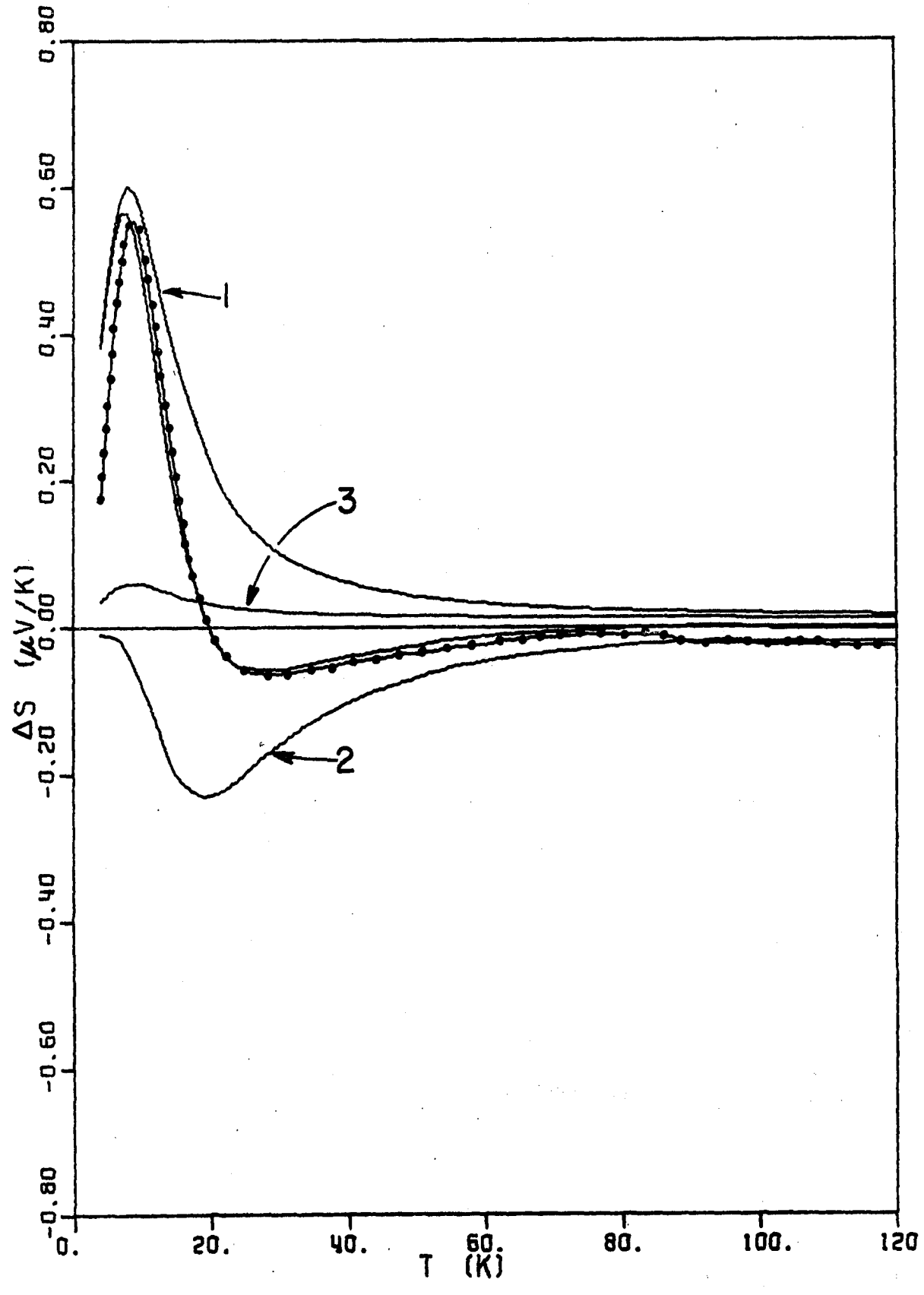
0.80
0.60
0.40
0.20
0.00
-0.20
-0.40
-0.60
-0.80
ΔS (μV/K)
0.
20.
40.
60.
80.
100.
120
T (K)
1
2
3

Figure 20. Thermopower of the Alloy In + 0.2 At. % Sn vs Pure Indium.

-•-• Measured data ΔS.

1. Calculated Nielsen-Taylor effect ΔS_e.
2. Calculated phonon drag effect ΔS_g.

—— Calculated total thermopower change: 1 + 2. (unlabelled)

3. Calculated diffusion thermopower without Nielsen-Taylor effect.

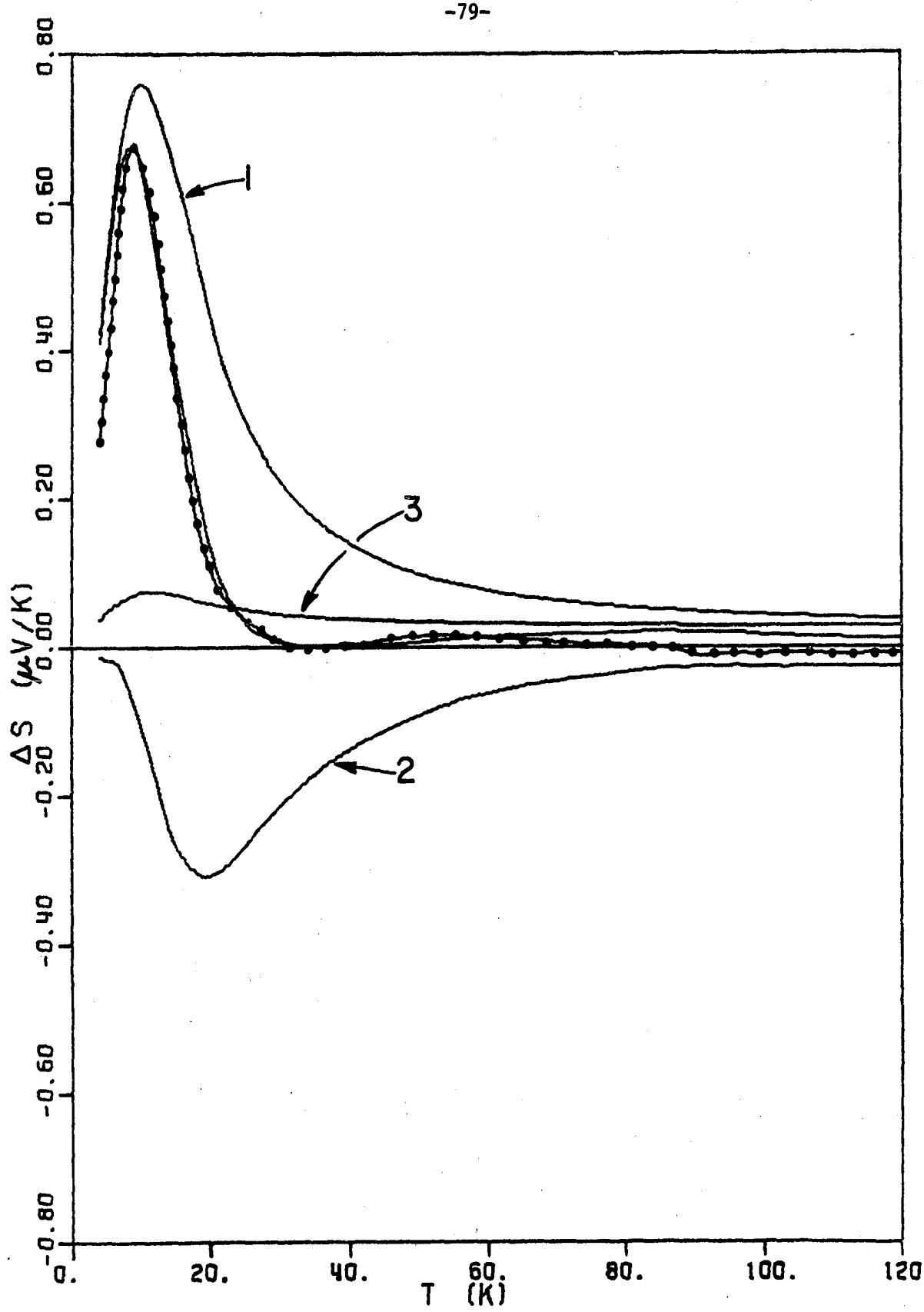
0.80
0.60
0.40
0.20
0.00
-0.20
-0.40
-0.60
-0.80
ΔS (μV/K)
0.
20.
40.
60.
80.
100.
120
T (K)
1
2
3

Figure 21. Thermopower of the Alloy In + 0.3 At. % Sn vs Pure Indium.

-●- Measured data ΔS.

1. Calculated Nielsen-Taylor effect ΔS_e.
2. Calculated phonon drag effect ΔS_g.

—— Calculated total thermopower change: 1 + 2. (unlabelled)

3. Calculated diffusion thermopower without Nielsen-Taylor effect.

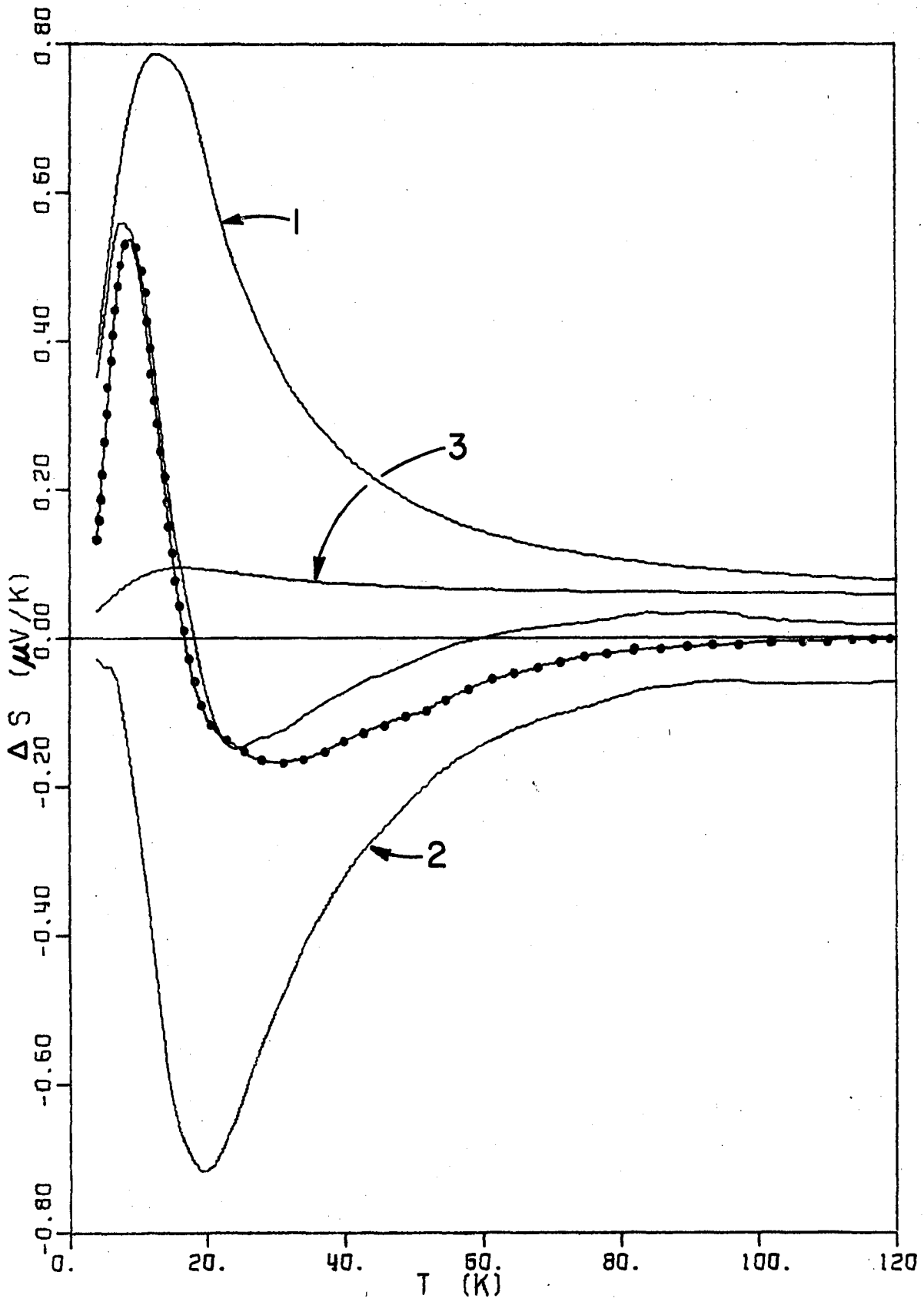
0.80
0.60
0.40
0.20
0.00
-0.20
-0.40
-0.60
-0.80
ΔS (μV/K)
0.
20.
40.
60.
80.
100.
120
T (K)
1
2
3

Figure 22. Thermopower of the Alloy In + 0.1 At. % Cd vs Pure Indium.

-●-● Measured data ΔS.

1. Calculated Nielsen-Taylor effect ΔS_e.
2. Calculated phonon drag effect ΔS_g.

—— Calculated total thermopower change: 1 + 2. (unlabelled)

3. Calculated diffusion thermopower without Nielsen-Taylor effect.

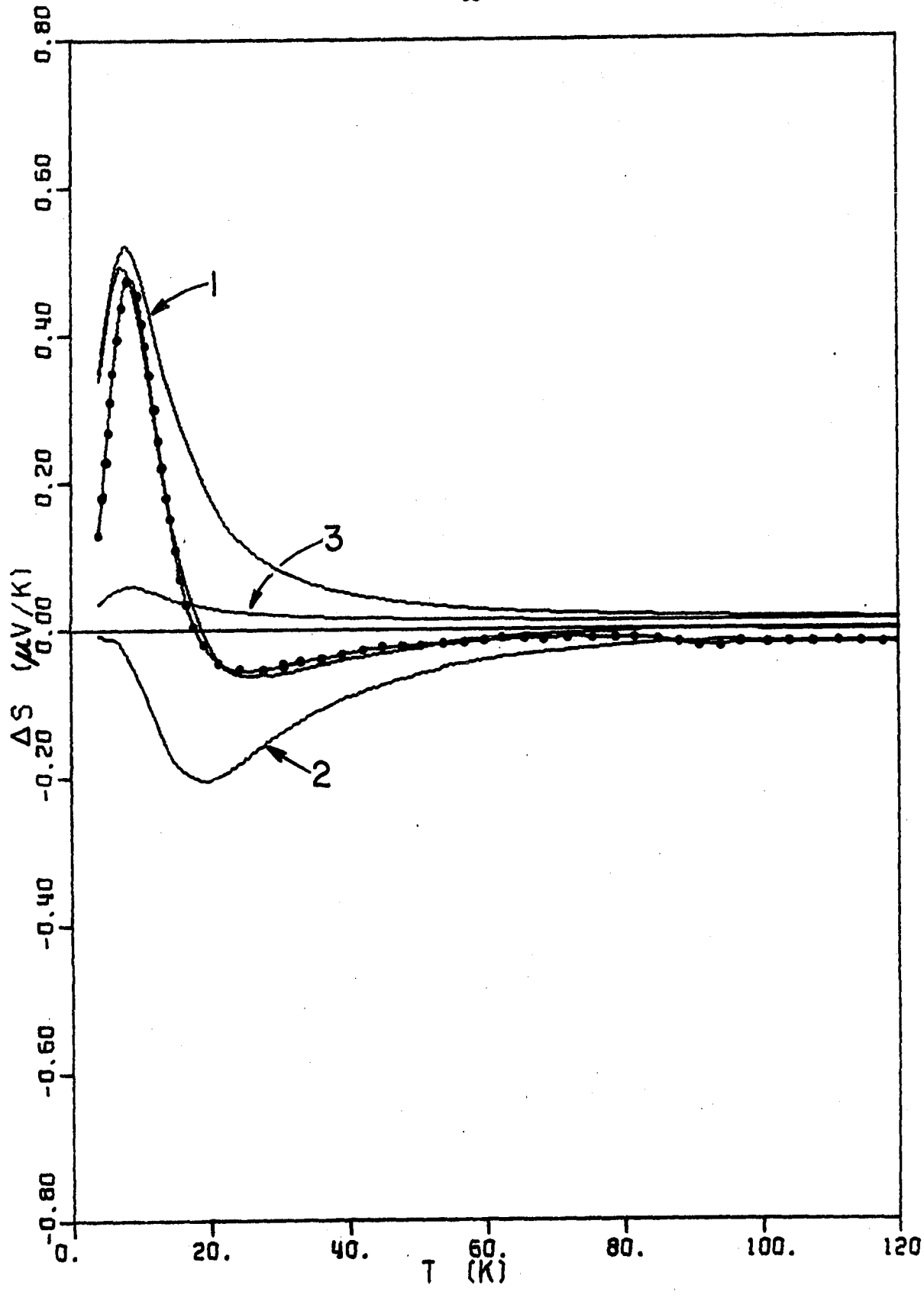
0.80
0.60
0.40
0.20
0.00
-0.20
-0.40
-0.60
-0.80
ΔS (μV/K)
0.
20.
40.
60.
80.
100.
120
T (K)
1
2
3

Figure 23. Thermopower of the Alloy In + 0.3 At. % Cd vs Pure Indium.

-●-● Measured data ΔS.

1. Calculated Nielsen-Taylor effect ΔS_e.
2. Calculated phonon drag effect ΔS_g.

—— Calculated total thermopower change: 1 + 2. (unlabelled)

3. Calculated diffusion thermopower without Nielsen-Taylor effect.

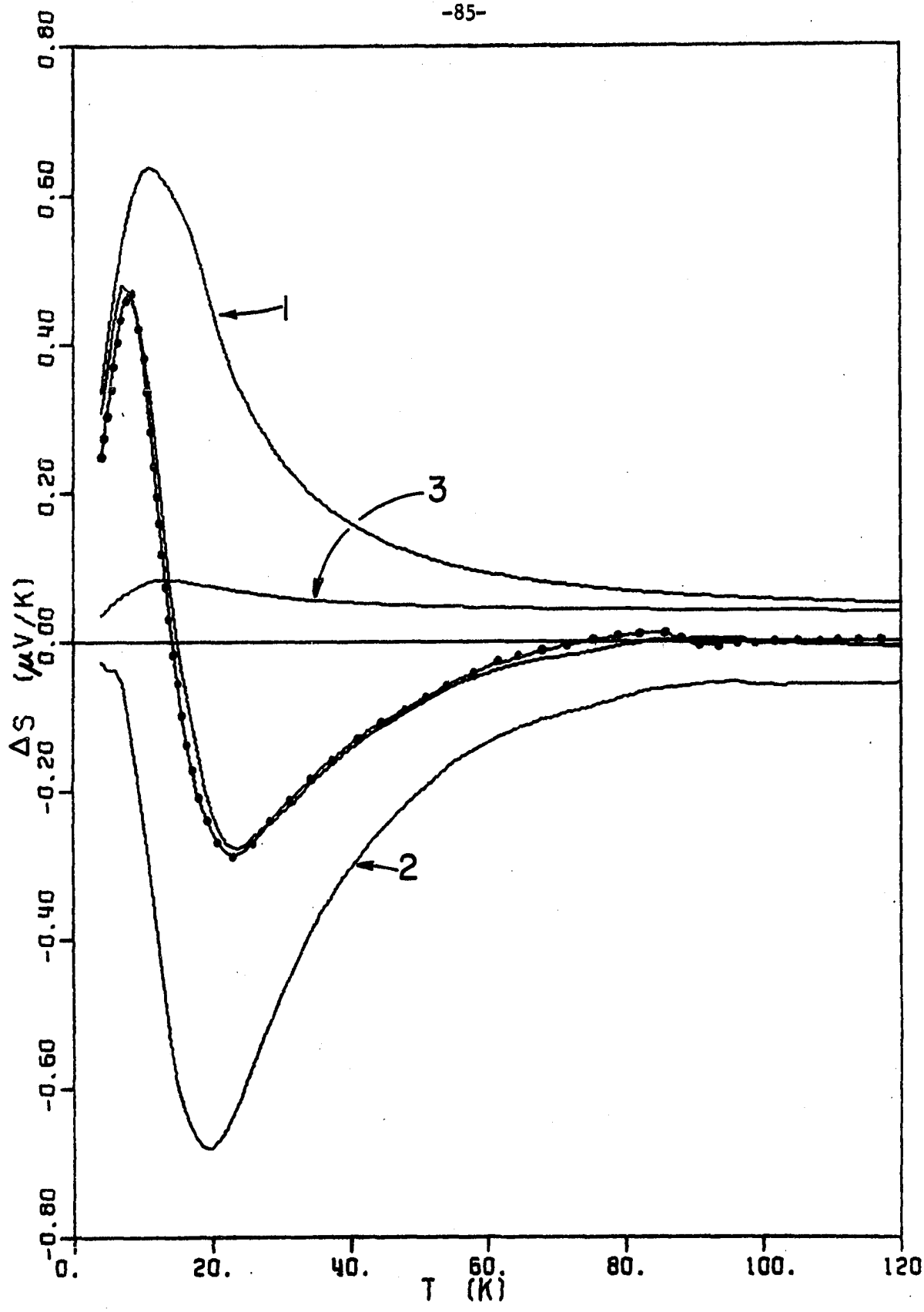
0.80
0.60
0.40
0.20
0.00
-0.20
-0.40
-0.60
-0.80
ΔS (μV/K)
0.
20.
40.
60.
80.
100.
120
T (K)
1
2
3

Figure 24. Thermopower of the Alloy In + 0.1 At. % Pb vs Pure Indium.

-●- Measured data ΔS.

1. Calculated Nielsen-Taylor effect ΔS_e.
2. Calculated phonon drag effect ΔS_g.

—— Calculated total thermopower change: 1 + 2. (unlabelled)

3. Calculated diffusion thermopower without Nielsen-Taylor effect.

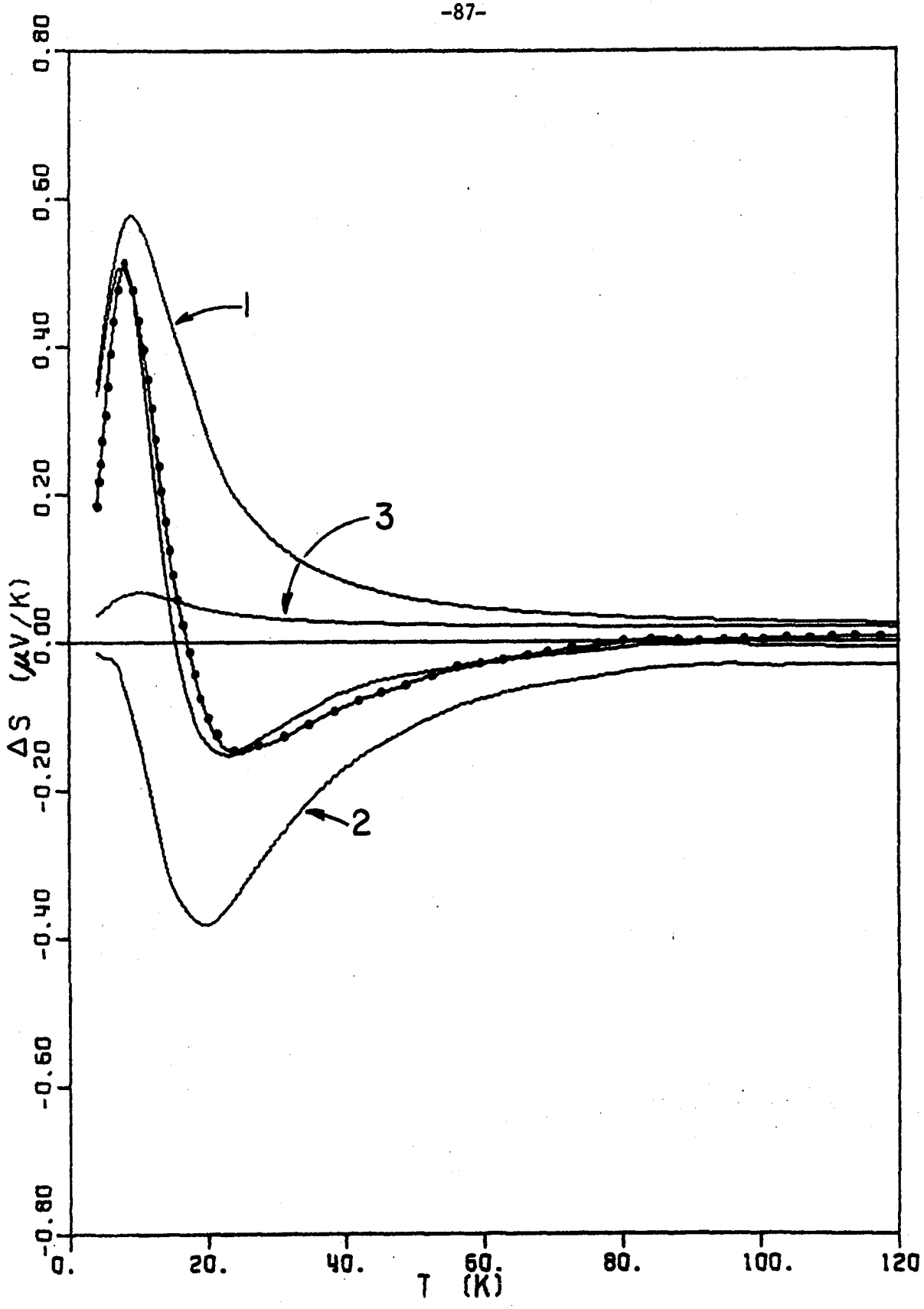
0.80
0.60
0.40
0.20
0.00
-0.20
-0.40
-0.60
-0.80
ΔS (μV/K)
0.
20.
40.
60.
80.
100.
120
T (K)
1
2
3

Figure 25. Thermopower of the Alloy In + 0.3 At. % Pb vs Pure Indium.

-●-● Measured data ΔS.

1. Calculated Nielsen-Taylor effect ΔS_e.
2. Calculated phonon drag effect ΔS_g.

—— Calculated total thermopower change: 1 + 2. (unlabelled)

3. Calculated diffusion thermopower without Nielsen-Taylor effect.

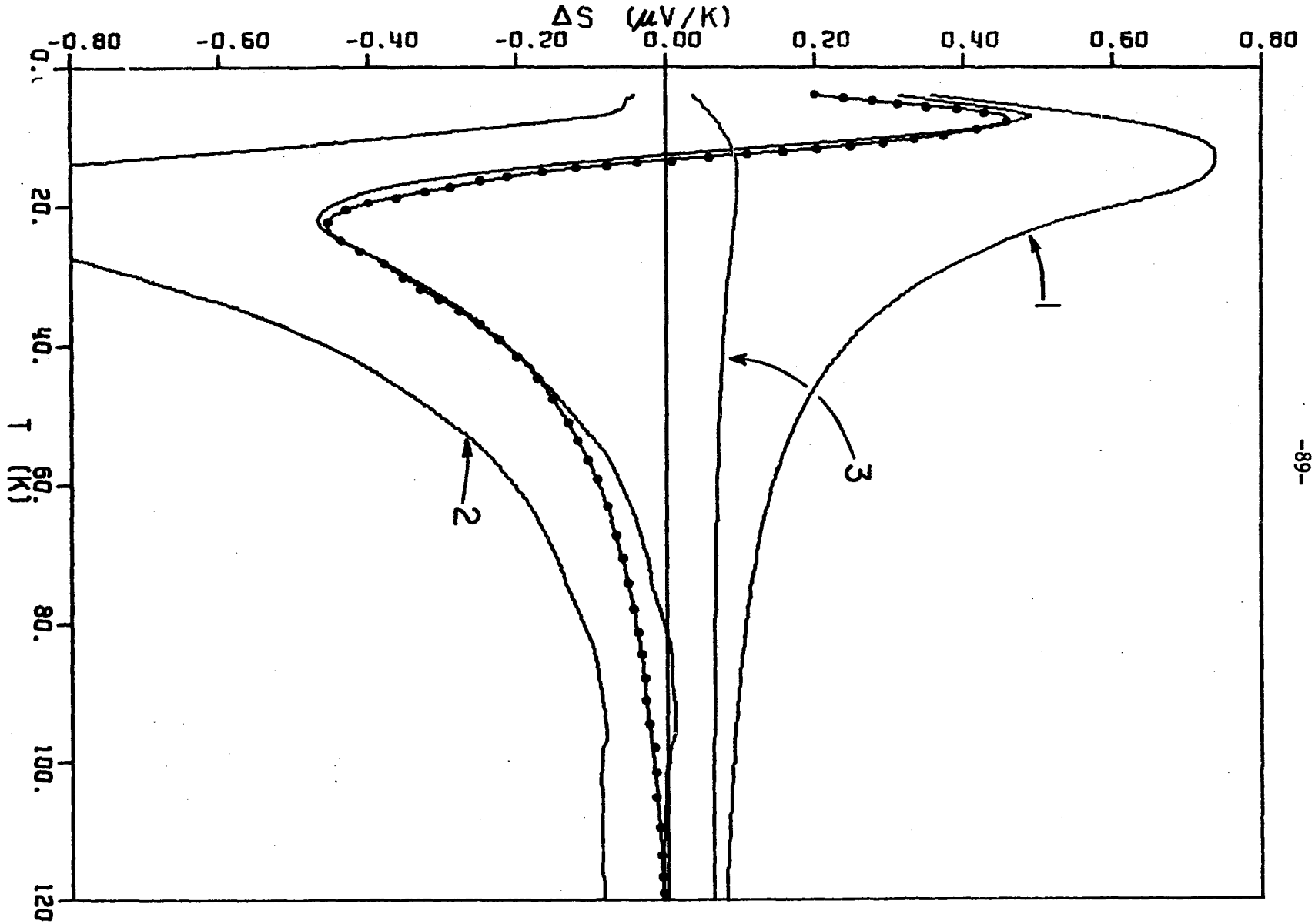
ΔS (μV/K)
-0.80
-0.60
-0.40
-0.20
0.00
0.20
0.40
0.60
0.80
T (K)
0.0
20.
40.
60.
80.
100.
120
1
2
3

Figure 26. Thermopower of the Alloy In + 0.1 At. % Ga vs Pure Indium.

-•- Measured data ΔS.

1. Calculated Nielsen-Taylor effect ΔS_e.
2. Calculated phonon drag effect ΔS_g.

—— Calculated total thermopower change: 1 + 2. (unlabelled)

3. Calculated diffusion thermopower without Nielsen-Taylor effect.

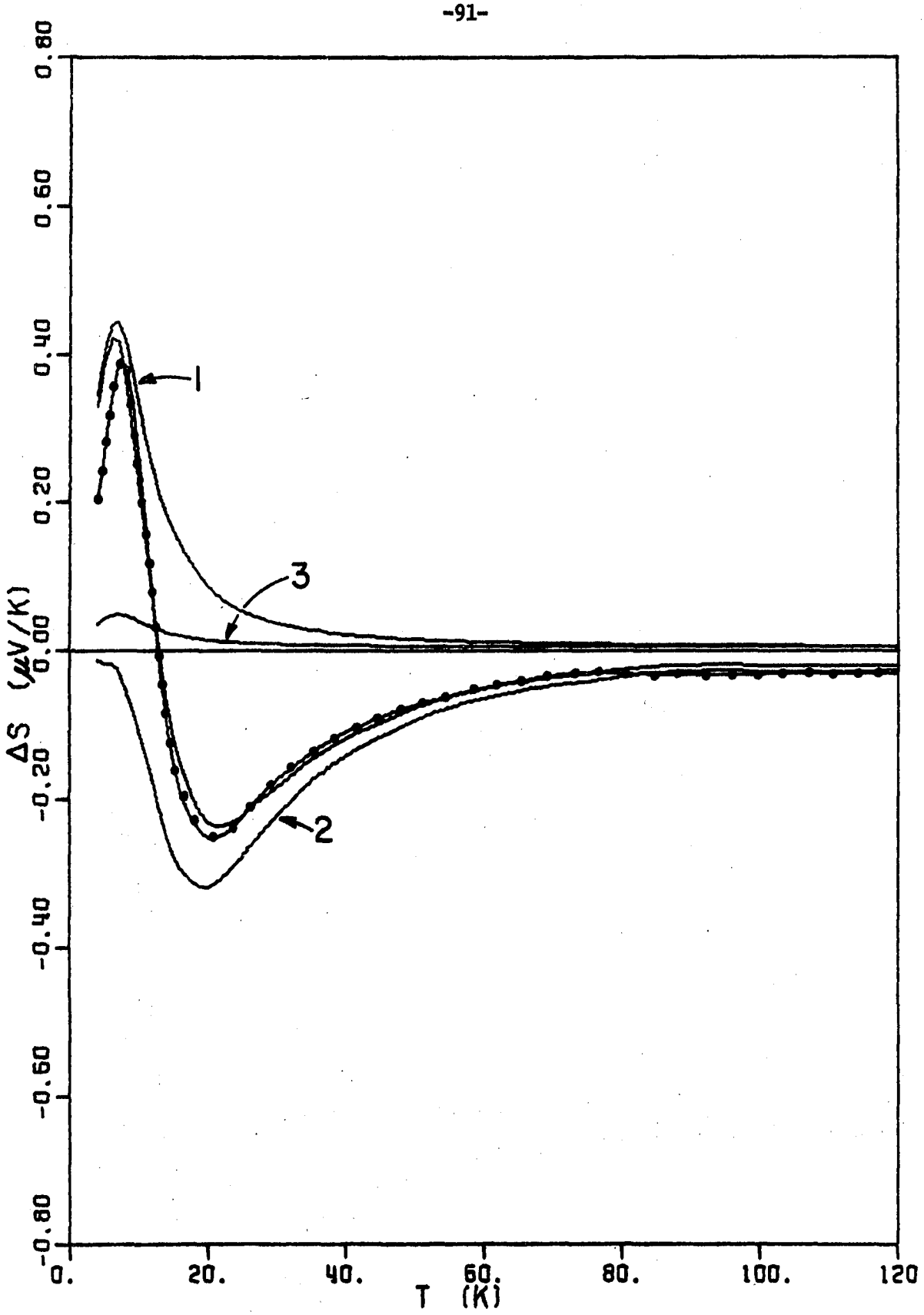
0.80
0.60
0.40
0.20
0.00
-0.20
-0.40
-0.60
-0.80
ΔS (μV/K)
1
2
3
0.
20.
40.
60.
80.
100.
120
T (K)

Figure 27. Thermopower of the Alloy In + 0.3 At. % Ga vs Pure Indium.

-•-•- Measured data ΔS.

1. Calculated Nielsen-Taylor effect ΔS_e.
2. Calculated phonon drag effect ΔS_g.

—— Calculated total thermopower change: 1 + 2. (unlabelled)

3. Calculated diffusion thermopower without Nielsen-Taylor effect.

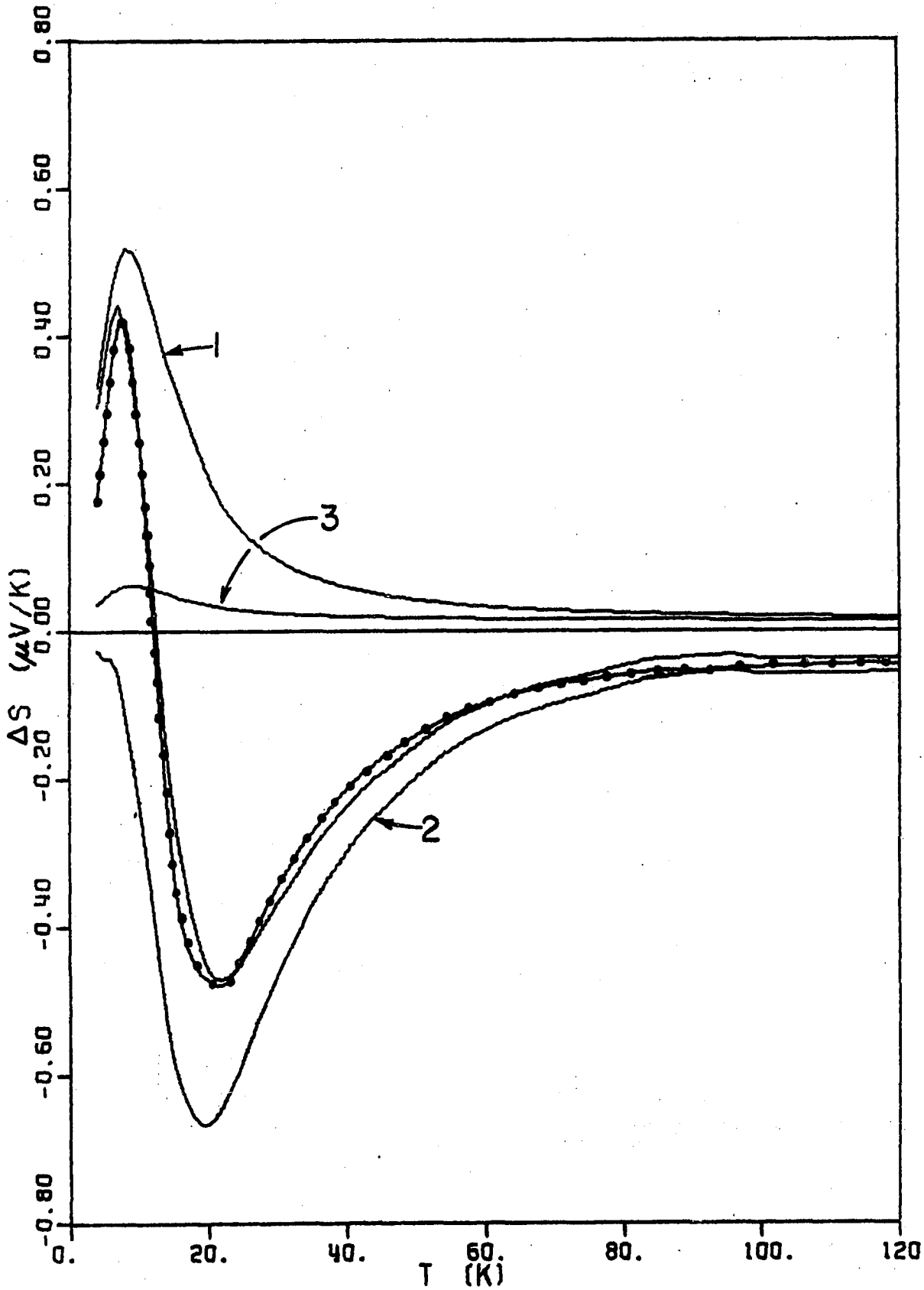
0.80
0.60
0.40
0.20
0.00
-0.20
-0.40
-0.60
-0.80
ΔS (μV/K)
1
2
3
0.
20.
40.
60.
80.
100.
120
T (K)

Figure 28. Thermopower of the Alloy In + 0.3 At. % Mg vs Pure Indium.

-●-● Measured data ΔS.

1. Calculated Nielsen-Taylor effect ΔS_e.
2. Calculated phonon drag effect ΔS_g.

—— Calculated total thermopower change: 1 + 2.

(unlabelled)

3. Calculated diffusion thermopower without Nielsen-Taylor effect.

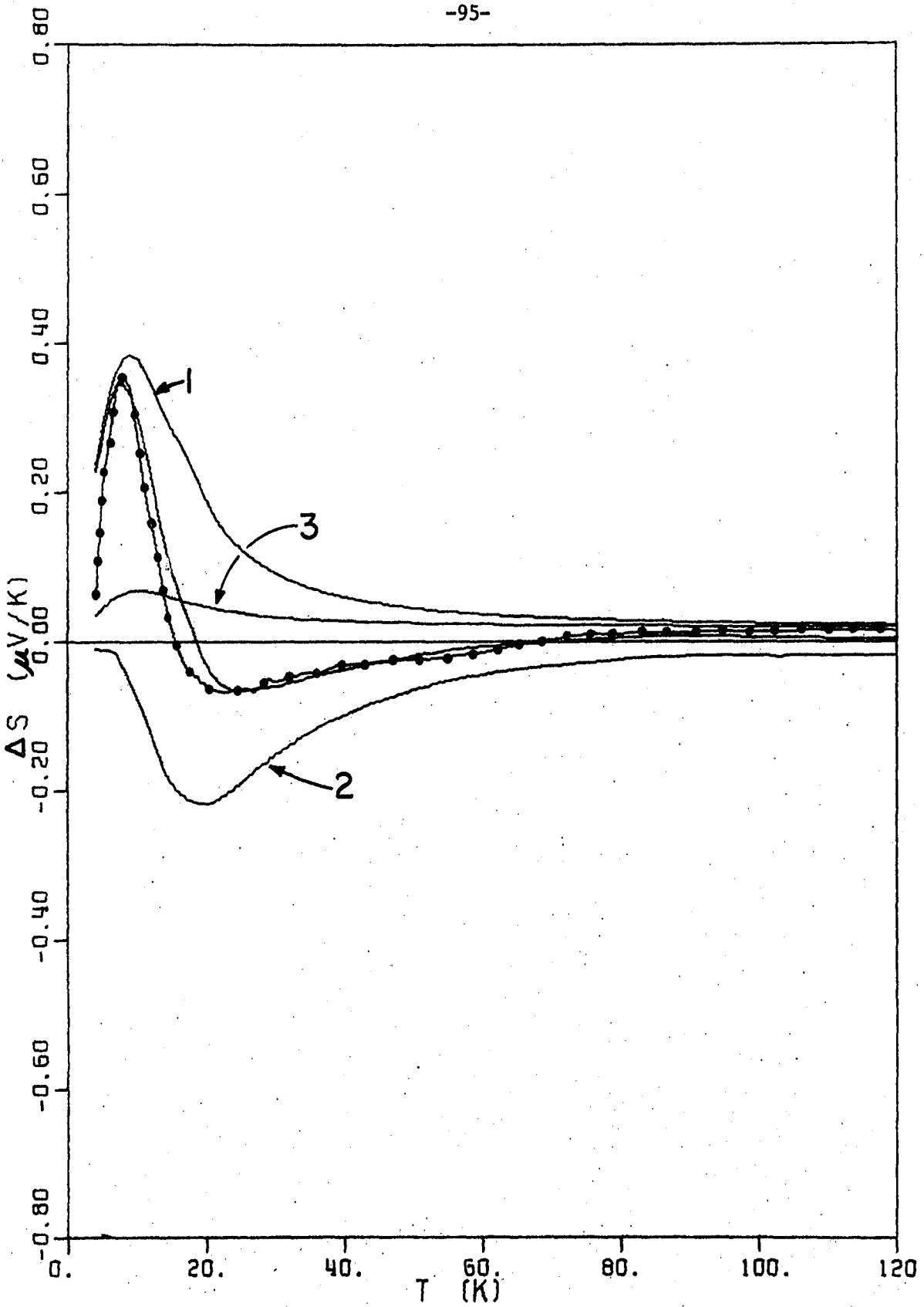
0.80
0.60
0.40
0.20
0.00
-0.20
-0.40
-0.60
-0.80
ΔS (μV/K)
0.
20.
40.
60.
80.
100.
120
T (K)
1
2
3

Figure 29. Thermopower of the Alloy In + 0.1 At. % Zn vs Pure Indium.

●—● Measured data ΔS.

1. Calculated Nielsen-Taylor effect ΔS_e.
2. Calculated phonon drag effect ΔS_g.

—— Calculated total thermopower change: 1 + 2.

(unlabelled)

3. Calculated diffusion thermopower without Nielsen-Taylor effect.

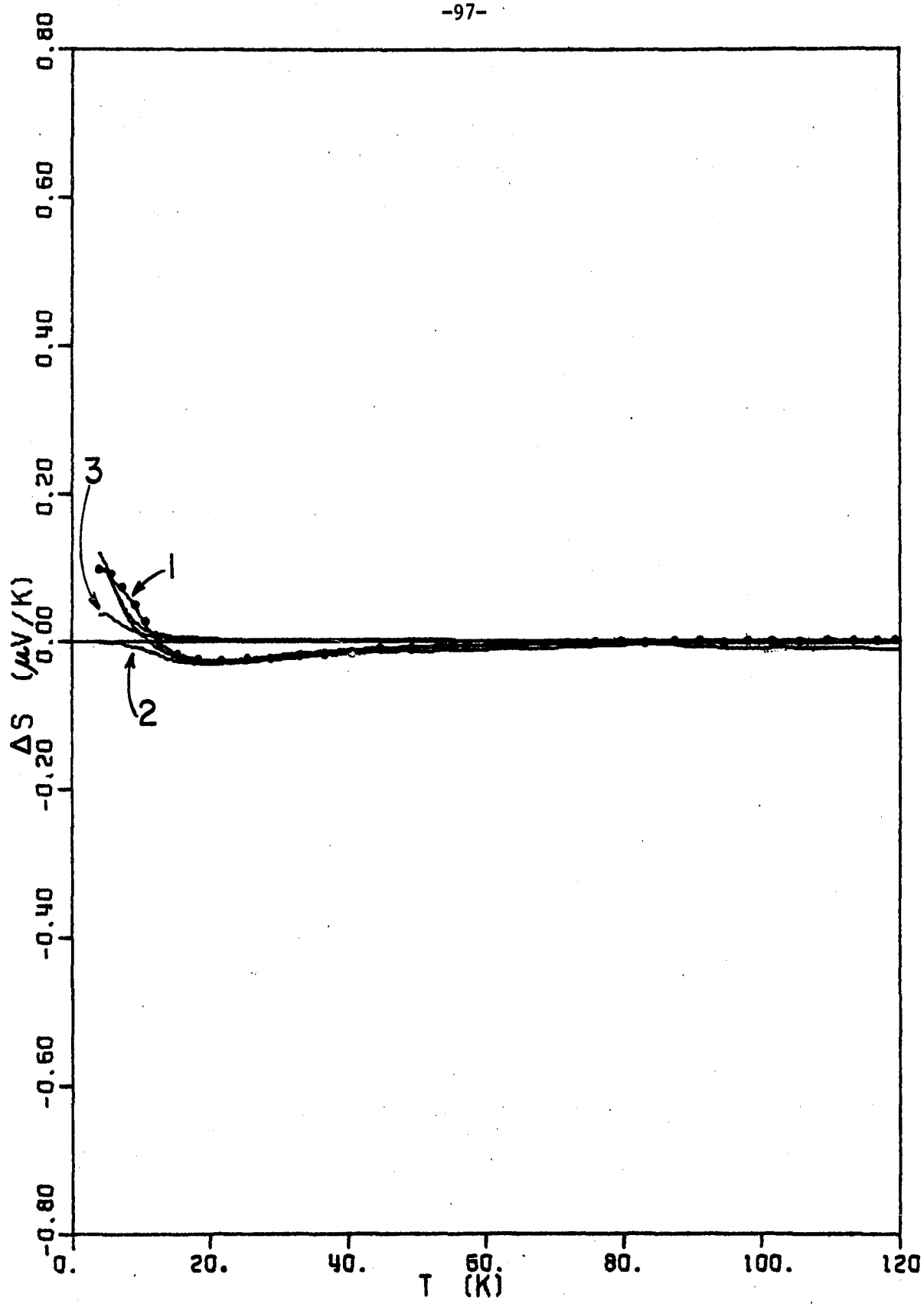
0.80
0.60
0.40
0.20
0.00
-0.20
-0.40
-0.60
-0.80
ΔS (μV/K)
0.
20.
40.
60.
80.
100.
120
T (K)
1
2
3

cedure outlined in Chapter II, Section I. Data shown in Figures 17, 21, 23, and 25 for 0.1% Th, 0.3% Sn, 0.3% Cd, and 0.3% Pb respectively have been adjusted and should not be given the same weight as the other data. This adjustment is discussed in Appendix A. At temperatures higher than 120 K the value of ΔS approaches zero, and this is not shown.

The graphs of ΔS vs T exhibit two main features in all the alloys: a negative peak at approximately 21 K and a positive peak at approximately 8 K. The negative peak represents a decrease of the thermopower of pure indium at 21 K. The positive peak corresponds to an increase in the thermopower which washes out the weak low temperature minimum of the pure indium thermopower curve (Figure 16).

B. Analysis of the Diffusion Component

The diffusion component of the thermopower change ΔS_e was analyzed in terms of Equation (27) which includes the Nielsen-Taylor corrections:

$$\Delta S_e = \frac{\rho_1}{\rho_o+\rho_1} Q[\xi_1+\Delta\xi_B+\Delta\xi_C-\xi_o-\Delta\xi_o]. \qquad (27)$$

The values used for each quantity are discussed below.

The quantity ξ_o is the first order themopower parameter for the pure metal. A theoretical expression for it, obtained by Nielsen and Taylor, is given in Equation (12). However, the logarithmic derivative in this equation is difficult to evaluate, so ξ_o is determined from the assumed linear function of temperature which represents

the first-order diffusion thermopower in the pure metal. In this situation $\xi_o = \xi$ in Equation (6). Then from Equations (6) and (7), one may write

$$\xi_o = \frac{3eE_F}{\pi^2 k_B^2} \frac{S_{oe}}{T} , \tag{41}$$

where S_{oe}/T is the slope of the straight line in Figure 16. The value used is $S_{oe}/T = 0.2 \times 10^{-8}$ $\mu V/K^2$. Conduction in polycrystalline indium is hole-like,[37] so the value of the carrier charge e was taken to be positive. The value of the Fermi energy E_F in indium is given in Table 1. The value of ξ_o obtained in this fashion is 0.71 and may be subject to as much as 100% error due to the uncertainty of the slope S_{oe}/T. However, this is not critical because ξ_o is overpowered by the other terms of Equation (27).

The pure metal Nielsen-Taylor correction $\Delta\xi_o$ is given by Equation (13). The mass ratio for indium was determined using the specific heat effective mass.[27] The function $\psi_1(\frac{T}{\theta})$ was obtained from a tabulation supplied by P. L. Taylor.[38] The "effective" pseudopotential V is a weighted average over appropriate values of the reduced phonon wave number $q/2k_F$. Bourassa and Dudenhoeffer[6] have obtained it in the context of a Debye model from the negative root of the expression

$$V^2 = \frac{\int_0^{x_o} |V_o(x)|^2 x^4 \operatorname{csch} (\frac{\theta}{T} \frac{x}{x_o}) dx}{\int_0^{x_o} x^4 \operatorname{csch} (\frac{\theta}{T} \frac{x}{x_o}) dx} \tag{42}$$

where $V_o(x)$ is the Animalu-Heine[27,39] pseudopotential form factor of the host, $x = q/2k_f$, and $x_o = q_o/2k_f$, with q_o the Debye cutoff wave vector. Obtained in this fashion, V turns out to be a weak function of temperature, ranging from a value of -0.382 ryd at 4 K to -0.90 ryd at 120 K in indium. Then $\Delta\xi_o$ ranges from -11.2 at 4 K to -0.1 at 120 K.

The first order impurity thermopower parameter ξ_1 is given by Equation (26). The logarithmic derivative is difficult to calculate. It should be on the order of unity, but its sign is uncertain.[3] A point-ion model was used to obtain the value -0.71 for this derivative. The details of this are carried out in Appendix B. Thus ξ_1 has the value 3.92.

The value of the second order impurity correction $\Delta\xi_C$ is obtained from Equation (25). The function $\psi_3(\frac{T}{\theta})$ was obtained from a tabulation provided by P. L. Taylor.[38] The value of $\Delta\xi_C$ ranges from -3.15 at 4 K to -0.05 at 120 K.

The term $\Delta\xi_B$ is given by Equation (24). The parameter U represents an "effective" pseudopotential difference between the impurity and the host. It is actually an extremely complex weighted average of actual pseudopotential form factors. Nielsen and Taylor[3] suggest an approximate form for U by assuming that the weighting factors can be ignored. Then U is given approximately by

$$U = \frac{\Omega_1}{\Omega_o} V_1(q) - V_o(q), \tag{43}$$

where Ω_1 and Ω_o are the impurity and host atomic volumes respectively, and where V_1 and V_o are values of the pseudopotentials of the impurity and host respectively evaluated at some "appropriate" value of the

phonon wave vector q. Nielsen and Taylor originally suggested taking $q = 0$, and this method has been used by Dudenhoeffer and Bourassa[5] in aluminum alloys. Meyer and Young[40] have suggested $q = (2/3)k_F$, and Bourassa and Dudenhoeffer[6] have used a similar criterion in their work on lead alloys. It is evident that this method can give, in general, no better than an order of magnitude estimate for U because the two values $V_1(q)$ and $V_o(q)$ are each relatively large and nearly equal. Thus the renormalization procedure is all important and yet the choice of the atomic volume ratio is an ad hoc assumption. In this work U has been treated as an adjustable constant in order to fit the sum of the Nielsen-Taylor prediction and the phonon drag prediction to the measured value of ΔS at the positive peak. The value of U should be of order 0.1 ryd[27] and should be independent of the concentration of impurity. The value of U obtained for each sample is listed in Table 4. Once U was determined for each alloy, then $\Delta\xi_B$ was calculated as a function of temperature from Equation (24). At low temperatures $\Delta\xi_B$ makes the greatest contribution to the term in brackets in Equation (27). For example, for the alloy In + 0.1 at. % Ga, $\Delta\xi_B = 19.02$ at 4 K. By 120 K its value has dropped to 0.81.

In summary the following can be said about the change in the diffusion thermopower parameter on alloying. The first-order change is given by $\xi_1 - \xi_o$, which has a value of 3.21 for all temperatures when calculated according to the models described above. The complete Nielsen-Taylor correction is $\Delta\xi_B + \Delta\xi_C - \Delta\xi_o$, the value of which is a function of temperature and is also dependent on the alloy. Its value for In + 0.1 at. % Ga, for example, ranges from 27.02 at 4 K to

Table 4. Fitting Parameters

Sample	$F=-\Delta S_g/S_g$	U (in ryd.)
*0.1 at. % Tl	0.16	0.13
0.3 at. % Tl	0.34	0.17
0.1 at. % Sn	0.13	0.16
0.2 at. % Sn	0.18	0.18
*0.3 at. % Sn	0.41	0.16
0.1 at. % Cd	0.12	0.14
*0.3 at. % Cd	0.39	0.13
0.1 at. % Pb	0.22	0.14
*0.3 at. % Pb	0.59	0.14
0.1 at. % Ga	0.18	0.13
0.3 at. % Ga	0.39	0.13
0.3 at. % Mg	0.13	0.07
0.1 at. % Zn	0.02	-0.02

*Indicates corrected data as explained in Appendix A.

0.89 at 120 K. So the Nielsen-Taylor second-order corrections to the change in the thermopower parameter dominate the first-order change at low temperatures.

The value of Q was obtained from Equation (7).

The value of ρ_1 for each alloy is listed in Table 3. The resistivity ρ_o of indium as a function of temperature was obtained from White and Woods.[41] The value for ρ_o at T = 295 K was taken as 8.8 μΩ-cm.

Finally ΔS_e was determined as a function of temperature from Equation (27). The results are the curves labelled 1 in Figures 17-29.

The result calculated for ΔS_e with the Nielsen-Taylor factors set equal to zero, i.e., $\Delta\xi_o = \Delta\xi_B = \Delta\xi_c = 0$, is shown as the curve labelled 3 in Figures 17-29.

C. Analysis of the Phonon Drag Component

The change ΔS_g in the phonon drag thermopower on alloying is given by Equation (40). This was fitted to the experimental data as follows. For each alloy it was assumed that

$$\frac{-\Delta S_g}{S_{og}} = F, \qquad 0 < T \lesssim \theta, \tag{44}$$

where F is a constant for a given alloy. At temperatures below the phonon drag peak, this assumption can be justified from Equations (33) and (38) if certain simplifying assumptions are made concerning the relaxation times τ_{pe}, τ_{pp}, and τ_l. At these low temperatures the phonon-electron interactions should dominate the phonon-phonon inter-

actions,[14] i.e.,

$$\frac{1}{\tau_{pe}} >> \frac{1}{\tau_{pp}} \tag{45}$$

It is also assumed that τ_{pe} is a constant over the entire temperature range $0<T\lesssim\theta$. From Equations (35) and (36) this implies that $\alpha_o(z)\sim 1$.

A pure Rayleigh Law is assumed to govern the phonon-impurity scattering,[14] i.e.,

$$\frac{1}{\tau_1} = a\omega^4 \tag{46}$$

where a is a constant. Then in terms of z,

$$\frac{1}{\tau_1} = aT^4\left(\frac{k_B}{\hbar}\right)^4 z^4 \tag{47}$$

Then Equation (40) can be written as follows

$$\Delta S_g = -A\left(\frac{T}{\theta}\right)^3 \int_0^{\frac{\theta}{T}} \frac{D(z)dz}{1+\dfrac{1}{\tau_{pe}aT^4\left(\frac{k_B}{\hbar}\right)^4 z^4}} \tag{48}$$

By the Mean Value Theorem of the First Kind[42] this can be written as

$$\Delta S_g = -A\left(\frac{T}{\theta}\right)^3 \frac{1}{1+\dfrac{1}{\tau_{pe}aT^4\left(\frac{k_B}{\hbar}\right)^4\gamma^4\left(\frac{\theta}{T}\right)^4}} \int_0^{\frac{\theta}{T}} D(z)dz \tag{49}$$

where γ is roughly constant and takes on some value $0\leq\gamma\leq 1$. This is assured by the fact that the integral is roughly constant as $\theta/T \to \infty$.

Therefore, the complex fractional coefficient of Equation (49) is very nearly independent of temperature. Equation (49) becomes

$$\Delta S_g = -F\, S_{og} \tag{50}$$

with $\alpha_o \sim 1$. This result is the same as the assumption of Equation (44).

Above the temperature of the phonon drag peak the phonon-phonon relaxation time τ_{pp} becomes dominant so that the simplifications above do not hold. The evaluation of Equation (40) for this case is complex, and the use of several unknown parameters cannot be avoided. In addition the choice of S_e/T which was arbitrarily made above begins to be important so that it is not possible to do any meaningful quantitative work at these higher temperatures. Thus the low temperature result of Equation (50) was assumed to be valid over the whole temperature range of 4 K to 120 K. The fraction F was used to fit the Nielsen-Taylor and phonon drag predictions to the measured data at 24 K. The resulting phonon drag prediction as a function of temperature is shown as curve 2 in Figures 17-29. Values obtained for F are listed in Table 4.

The two adjustable parameters U and F can change only the heights of the Nielsen-Taylor curve and the phonon drag curve. They were varied self-consistently so that the total predicted thermopower curve (the sum of the Nielsen-Taylor curve 1 and the phonon drag curve 2) fitted the measured data at the positive peak and at 24 K.

V. DISCUSSION AND CONCLUSIONS

A. Discussion of Thermopower Results

The total predicted thermopower change on alloying is shown in Figures 17-29 as the solid unlabelled line. It is obtained by adding the calculated Nielsen-Taylor curve (labelled 1) and the calculated phonon-drag curve (labelled 2). (Curve 3 gives the change in the diffusion component, uncorrected for the Nielsen-Taylor effect.)

The Nielsen-Taylor corrections to the diffusion thermopower are dominant at low temperatures. This is easily seen by comparing curve 1 with curve 3 in Figures 17-29. It should be noted that the large peak in the Nielsen-Taylor curves is not due entirely to the Nielsen-Taylor correction terms, as a much lower peak is also seen in the uncorrected diffusion curve. This is due to the factor $\rho_1/(\rho_o+\rho_1)$ in Equation (27), which also has a maximum at approximately 10 K, regardless of the Nielsen-Taylor terms.

The fitted values of the pseudopotential U (Table 4) are of the correct order of magnitude, which can be seen by comparing them to the theoretical pseudopotential values of Animalu and Heine.[27,39] However, they do not show the variations in sign for different impurities that might be expected for a quantity that is some effective difference in pseudopotential between host and impurity. For the most part the

fitted values of U are independent of concentration for a particular impurity, which is to be expected.

The fact that the value of the phonon drag fitting parameter F is less than one for each alloy is consistent with the assumption that the minimum at 21 K in the alloy data represents a depression of the phonon drag peak on alloying. This can be seen from the analysis leading up to Equation (50), which indicates that F is less than one. The fact that F increases with increasing concentration is consistent with the basic idea of phonon drag which is that alloying gives the phonons something extra to scatter from, reducing the percentage of electron-phonon interactions and thus decreasing the magnitude of the phonon drag peak. One expects the reduction to be greater as the amount of impurity is increased.

The fraction F can be used to investigate the Rayleigh scattering parameter a, which depends on the type of impurity present and its concentration c.[14] Equations (49) and (50) imply that

$$F = \frac{1}{1 + \frac{1}{a\tau_{pe}\gamma^4 (\frac{k_B\theta}{\hbar})^4}} \qquad (51)$$

The analysis does not include a method for determining the absolute value of a; however, relative magnitudes can be calculated as follows. The Rayleigh scattering parameter was arbitrarily chosen to have the value a_o in the alloy In + 0.1 at. % Ga. Then the relative value a/a_o was calculated for each alloy using the values of F from Table 4 in conjunction with Equation (51). The ratio $(a/c)/(a_o/c_o)$, where c_o is the impurity concentration in the In + 0.1 at. % Ga alloy, was

also determined. The results are listed in Table 5.

It is seen that the relative parameter a/a_o is roughly proportional to the impurity concentration for the solutes thallium, gallium, and to a lesser extent tin. The departure from proportionality for cadmium and lead may be due to inaccuracies introduced in adjusting the thermoelectric data to account for behavior due to factors other than the impurity.

The change in the thermopower of indium on alloying is not easily explained solely on the basis of the Nielsen-Taylor theory or solely on the basis of phonon drag. But an additive combination of the two yields an excellent fit to the experimental data for each alloy.

The low temperature peak seen in each thermopower curve (Figures 17-29) corresponds to an increase in the thermopower on alloying. The usual view of this anomaly is that it too is a phonon drag effect. Dugdale and Bailyn[43] have suggested that the contribution to S_{og} from the various parts of the Fermi surface differ greatly in both magnitude and sign. They point out that, if the electron-phonon scattering and the electron-impurity scattering vary differently over the Fermi surface, it would be possible to have phonon drag enhancement at low temperatures. Huebener[30] has used this idea to discuss the results of his thermopower work on dilute aluminum alloys. However, at this time no work has been done to develop this into a quantitative theory.

It is suggested that it is not necessary at this point to rely on what is still a qualitative phonon drag theory to explain the low-temperature enhancement of the thermopower in indium and aluminum[5]

Table 5. Calculated Rayleigh Scattering Parameter Ratios

Sample	a/a_o	$(a/c)/(a_o/c_o)$
*0.1 at. % Tl	0.86	0.86
0.3 at. % Tl	2.36	0.79
0.1 at. % Sn	0.58	0.58
0.2 at. % Sn	1.00	0.50
*0.3 at. % Sn	3.14	1.05
0.1 at. % Cd	0.54	0.54
*0.3 at. % Cd	2.91	0.97
0.1 at. % Pb	1.27	1.27
*0.3 at. % Pb	5.55	1.85
0.1 at. % Ga	1.00	1.00
0.3 at. % Ga	2.91	0.97
0.1 at. % Mg	0.58	0.58
0.1 at. % Zn	0.09	0.09

a_o has been chosen arbitrarily as the scattering parameter for a concentration c_o of 0.1 At. % Ga.

* Indicates corrected data as explained in Appendix A.

alloys. Both cases are reasonably well explained by the Nielsen-Taylor diffusion theory.

B. Sources of Error

The precision with which thermoelectric potential measurements could be made was affected by several factors. The potentiometer readings could be easily repeated to ± 0.005 μV if the voltage was steady. This was generally the situation below approximately 40 K where the temperature controller functioned best. At 80 K (using a liquid helium bath) the readings could be repeated typically to ± 0.03 μV for the specimen thermocouples.

There was always a small spurious thermoelectric potential present due to inhomogenieties in the copper leads running from the cryogenic bath to room temperature. This was on the order of 0.5 μV for liquid helium and 0.1 μV for liquidnitrogen. Especially in liquid helium, this spurious background potential was a weak function of time as the level of liquid fell. Over the period of one complete cycle comprised of an up-run and a down-run (approximately seven hours), the background could change by as much as 0.2 μV, although generally the change was less. But over the much shorter time period (approximately 30 minutes) required to take the data points for the cluster fitting procedure used, the background was in general essentially constant and therefore had negligible effect on the calculation of the thermopower.

The temperature of the heat sink was measured over the temperature range of the liquid helium run from 4.2 K to 100 K. When

the hot junction of the specimen thermocouple was at 100 K, the heat sink temperature had drifted upward only 0.1 K. So this was neglected.

The error in the measurement of the temperature has already been discussed to some extent in Chapter II, Section G. The error at high temperatures was greater because of the longer times required for the heater block to achieve equilibrium. So the .02 K error at 77 K mentioned previously is possibly too small, as it was obtained at equilibrium in liquid nitrogen. An estimate of the maximum error in this temperature region is ± 0.1 K. The maximum error of ± 0.05 K at 7.25 K was determined under dynamic conditions previously explained. So this is retained as a maximum error in the absolute temperature measurement at very low temperatures.

The uncertainty in the thermopower difference ΔS can be gauged simply in the following manner. The approximation

$$\Delta S \simeq \frac{\Delta V}{\Delta T} \tag{52}$$

can be made, where ΔV is the measured change in thermoelectric potential corresponding to a change in temperature ΔT. To first order the uncertainties in the measured quantities propagate as

$$\delta(\Delta S) \simeq \frac{\Delta V}{(\Delta T)^2}\,\delta(\Delta T) + \frac{\delta(\Delta V)}{\Delta T}\ , \tag{53}$$

where δ represents the error in the quantity enclosed in parentheses. The estimated maximum uncertainties in V and T are given above. Equation (53) involves uncertainties in differences, however. The difference

in the temperature is known to approximately 10^{-4} K at low temperatures and 10^{-3} K at higher temperatures, which makes the first term on the right side of Equation (53) negligible. The worst value for $\delta(\Delta V)$ exists if the uncertainties in V add when the difference is taken, i.e., $\delta(\Delta V) = 2\delta(V)$. Assuming this to be the case, one obtains from Equation (53) the following typical values:

$$\delta(\Delta S) = \pm 0.02\ \mu V/K \text{ at } 8.0\ K;$$

$$\delta(\Delta S) = \pm 0.01\ \mu V/K \text{ at } 80\ K.$$

The scatter in the calculated values of ΔS indicates that these uncertainties are essentially correct.

APPENDIX A

Most of the specimens supplied by Cominco American, Inc. gave results that were clearly not due to impurities alone. These specimens are marked by an asterisk in Table 4. The characteristic feature of their thermopower curves is evident in Figure A1, which shows the measured thermopower of 0.3 at. % Sn versus pure indium (solid curve). The value of ΔS at high temperatures is not small, as it should be, and in fact is increasing in magnitude. This is probably due to a preferential direction of crystal growth during the extrusion process. Thus there is a difference between the thermopower of the alloy and the pure metal which is not due to impurities, but due to the fact that the thermopower of indium is not isotropic. To correct for this effect a term ΔS_{corr} was added to each of the four data sets, where

$$\Delta S_{corr} = AT + B. \tag{A1}$$

The constants A and B were determined to make the data go to zero at high temperatures. Figure A1 shows ΔS_{corr} for 0.3 at. % Sn (dashed line).

This method is, of course, arbitrary and one would be forced to throw out this data if quantitative results were to be obtained. However, the corrected curves certainly show the major features of

Figure A1. Graph of ΔS of In + 0.3 Atomic % Sn vs In Showing Correction Factor.

Full curve: Measured thermopower.

Dashed curve: Correction factor.

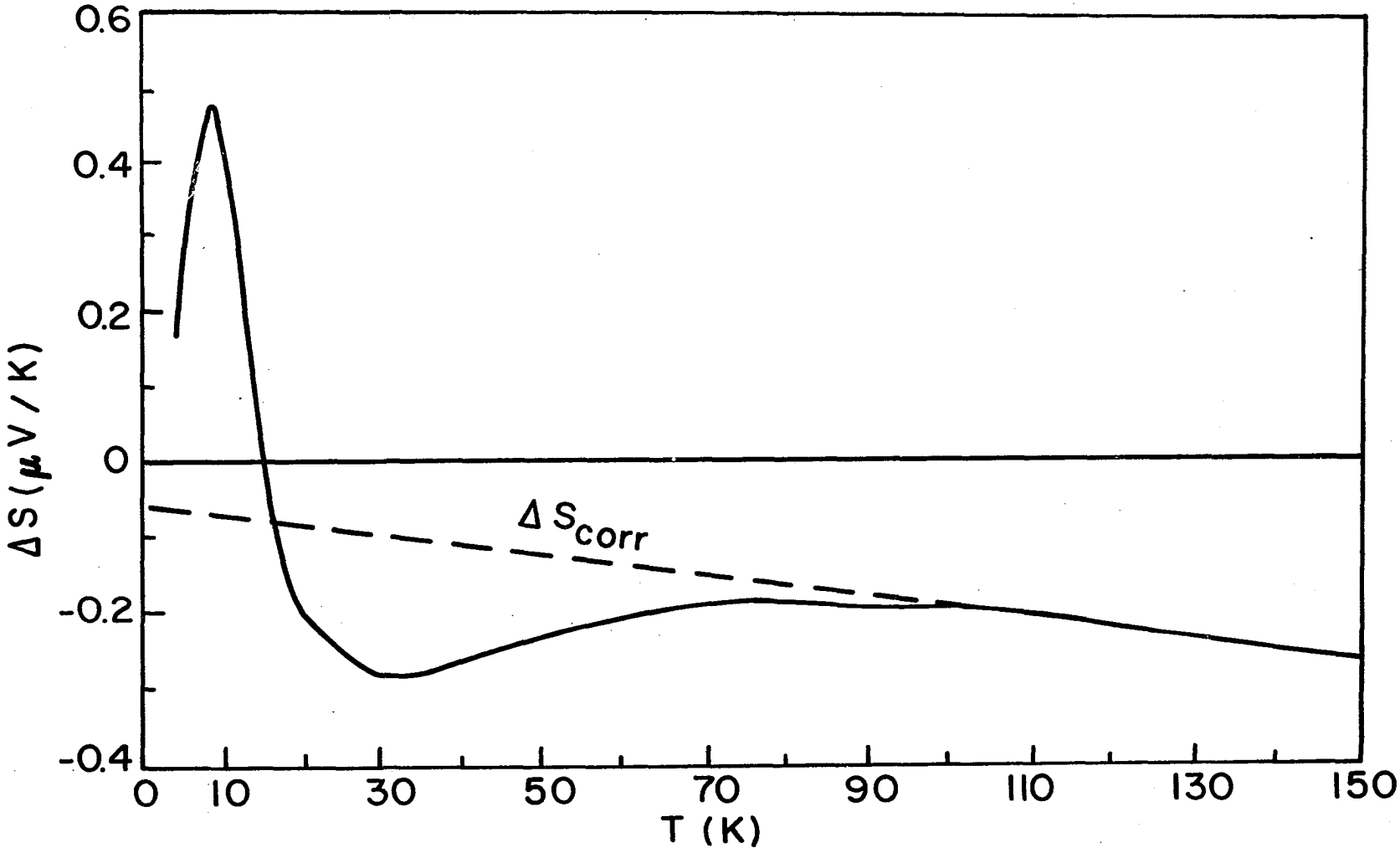
0.6
0.4
0.2
0
-0.2
-0.4
ΔS (μV / K)
ΔS corr
0
10
30
50
70
90
110
130
150
T (K)

the effect of impurities and for that reason are included. It is clear, of course, that the errors in the four sets of adjusted data involved are substantially larger than the errors for the other nine data sets.

APPENDIX B

In a metal the potential created by a substitutional impurity can be written as

$$U(q) = U_o(q)/\chi(q), \tag{B1}$$

where q is the magnitude of the phonon wave vector, $U_o(q)$ is the potential at the affected site, and $\chi(q)$ is the Hartree dielectric constant which accounts for crystal effects.

The simplest assumption for $U_o(q)$ is a point-ion approximation,

$$U_o(q) = \frac{4\pi e^2}{q^2}. \tag{B2}$$

Thus
$$\frac{\partial \ln U(q)}{\partial \ln \varepsilon} = -\frac{\partial \ln q^2}{\partial \ln \varepsilon} + \frac{\partial \ln \chi(q)}{\partial \ln \varepsilon}, \tag{B3}$$

but
$$q^2 = 2k^2(1-\cos^2\theta), \tag{B4}$$

and
$$\varepsilon = k^2 \text{ (in atomic units)}, \tag{B5}$$

so
$$\frac{\partial \ln q^2}{\partial \ln \varepsilon} = 1. \tag{B6}$$

The dielectric constant is given by

$$\chi(q) = 1 + \frac{\lambda^2}{q^2}\left[\frac{1}{2} + \frac{4k^2-q^2}{4kq} \ln\left|\frac{2k+q}{2k-q}\right|\right], \tag{B7}$$

where $$\lambda^2 = 4\pi e^2 N(\varepsilon),$$

and $N(\varepsilon)$ = the density of states function

$N(\varepsilon)$ is proportional to $\varepsilon^{1/2}$, so

$$\frac{\partial \lambda^2}{\partial \varepsilon} = \frac{\lambda^2}{2\varepsilon} . \tag{B8}$$

Using Equations (B5)-(B8), one derives

$$\frac{\partial \ln \chi(q)}{\partial \ln \varepsilon} = - \frac{[\chi(q)-1]}{2\chi(q)} . \tag{B9}$$

This can be combined with Equations (B3) and (B6) to give

$$\frac{\partial \ln U(q)}{\partial n \varepsilon} = - \frac{1}{2} - \frac{1}{2\chi(q)} . \tag{B10}$$

Values of the Hartree dielectric constant for indium as a function of q can be determined following Harrison.[27] The value of $\frac{\partial \ln U(q)}{\partial \ln \varepsilon}$ used in the analysis of Chapter IV is the average value over all q from zero to $2k_F$.

LIST OF REFERENCES

1. P. E. Nielsen and P. L. Taylor, Phys. Rev. Lett. 21, 893 (1968).
2. P. E. Nielsen and P. L. Taylor, Phys. Rev. Lett. 25, 371 (1970).
3. P. E. Nielsen and P. L. Taylor, A. E. C. Technical Report No. 65 (COO-623-152), 1970 (unpublished).
4. P. E. Nielsen and P. L. Taylor (unpublished).
5. A. W. Dudenhoeffer and R. R. Bourassa, Phys. Rev. B5, 1651 (1972).
6. R. R. Bourassa and A. W. Dudenhoeffer, Phys. Rev. B7, 1270 (1973).
7. T. Rybka and R. R. Bourassa, Phys. Rev. B8, 4449 (1973).
8. D. K. C. MacDonald, Thermoelectricity: An Introduction to the Principles. Wiley, New York, 1962.
9. R. P. Huebener, Solid State Phys. 27, 63 (1973).
10. J. Kondo, Progr. Theoret. Phys. 32, 37 (1964).
11. M. Barisoni, R. K. Williams, and D. L. McElroy, Proc. 7th Conf. on Thermal Conductivity (1968).
12. B. Bosacchi and R. P. Huebener, J. Phys. F: Metal Phys., 1, L27 (1971).
13. T. W. Rybka, dissertation, Univ. of Okla., 1973, (unpublished).
14. R. P. Huebener, Phys. Rev. 146, 490 (1966).
15. A. C. Anderson, Rev. of Sci. Inst., 39, 605 (1968).
16. G. K. White, Experimental Techniques in Low-Temperature Physics, 2nd Ed., Oxford, 1968.
17. R. P. Ries and B. K. Moore, Rev. of Sci. Inst., 41, 996 (1970).

18. R. F. Moreland, dissertation, Univ. of Okla., 1974 (unpublished).

19. G. Cataland and H. H. Plumb, J. Res. of N.B.S., 70A, 178-243 (1966).

20. J. E. Nicholson, dissertation, Univ. of Okla., 1972 (unpublished).

21. C. Dasarathy, Z. Metall Kunde, Bd. 61, 121 (1970).

22. N. F. Mott and H. Jones, The Theory of the Properties of Metals and Alloys, Dover, 1958.

23. J. M. Ziman, Electrons and Phonons, Oxford, 1960.

24. P. L. Taylor, A Quantum Approach to the Solid State, Prentice-Hall, 1970.

25. P. L. Taylor, Proc. Roy. Soc. A275, 200 (1963).

26. A. B. Migdal, Zh. Eksp. Teor. Fiz., 34, 1438 (1958).

27. W. A. Harrison, Pseudopotentials in the Theory of Metals, Benjamin, 1966.

28. J. A. Moriarty, Phys. Rev., B1, 1363 (1970).

29. American Institute of Physics Handbook, Third Edition, D. E. Gray, Ed., McGraw-Hill, 1972.

30. R. P. Huebener, Phys. Rev., 171, 634 (1968).

31. M. Bailyn, Phil. Mag., 5, 1059 (1960).

32. A. V. Gold and W. B. Pearson, Can. J. Phys., 39, 445 (1961).

33. A. R. DeVroomen, C. Van Baarle, and A. J. Cuelenaere, Physica, 26, 19 (1960).

34. I. I. Hanna and E. H. Sondheimer, Proc. Roy. Soc., A239, 247 (1957).

35. R. P. Huebener, Phys. Rev., A135, 1281 (1964).

36. J. W. Christian, J. P. Jan, W. B. Pearson, and I. M. Templeton, Proc. Roy. Soc. (London) A246, 213 (1958).

37. R. Lück, Phys. Stat. Solidi 18, 49 (1966).

38. P. L. Taylor (private communication).

39. A. E. O. Animalu and V. Heine, Phil. Mag., 12, 1249 (1965).

40. A. Meyer and W. H. Young, Phys. Rev. 184, 1003 (1969).

41. G. K. White and S. B. Woods, Rev. Sci. Instr. 28, 638 (1957).

42. F. B. Hildebrand, Introduction to Numerical Analysis (McGraw Hill Inc., New York, 1956).

43. J. S. Dugdale and M. Bailyn, Phys. Rev. 157, 485 (1967).